Classical density functional theory for the prediction of the surface tension and interfacial properties of fluids mixtures of chain molecules based on the statistical associating fluid theory for potentials of variable range

Fèlix Llovell,[1] Amparo Galindo,[1] Felipe J. Blas,[2] and George Jackson[1,a)]
[1]*Department of Chemical Engineering, Imperial College London, South Kensington Campus, SW7 2AZ London, United Kingdom*
[2]*Departamento de Física Aplicada, Facultad de Ciencias Experimentales, Universidad de Huelva, 21071 Huelva, Spain*

(Received 10 March 2010; accepted 19 May 2010; published online 14 July 2010)

The statistical associating fluid theory for attractive potentials of variable range (SAFT-VR) density functional theory (DFT) developed by [G. J. Gloor *et al.*, J. Chem. Phys. **121**, 12740 (2004)] is revisited and generalized to treat mixtures. The Helmholtz free-energy functional, which is based on the SAFT-VR approach for homogeneous fluids, is constructed by partitioning the free-energy density into a reference term (which incorporates all of the short-range interactions and is treated locally) and an attractive perturbation (which incorporates the long-range dispersion interactions). In this work, two different functionals are compared. In the first, one uses a mean-field version of the theory to treat the long-range dispersive interaction, incorporating an approximate treatment of the effect of the correlations on the attractive energy between the segments by introducing a short-range attractive contribution in the reference term. In the second, one approximates the correlation function of the molecular segments in the inhomogeneous system with that of a homogeneous system for an average density of the two positions, following the ideas proposed by Toxvaerd [S. Toxvaerd, J. Chem. Phys. **64**, 2863 (1976)]. The SAFT-VR DFT formalism is then used to study interfacial properties and adsorption phenomena at the interface. A detailed analysis of the influence of the molecular parameters on the surface tension and density/composition profiles of the mixtures is undertaken for binary mixtures of molecules of different chain length, segment diameter, dispersive energy, and attractive range. The effect of the asymmetry of the molecular species on the adsorption phenomena is examined in some depth. The adequacy of the approach is demonstrated by comparing the theoretical predictions with the interfacial properties of some real mixtures. The relative merits of the two approximate free-energy functionals are assessed by examining the vapor-liquid interfacial tension of selected mixtures of *n*-alkanes. The theory generally provides an excellent description of the interfacial properties of the mixtures without the need for further adjustment of intermolecular parameters obtained from an examination of the bulk fluid-phase behavior alone. © *2010 American Institute of Physics*. [doi:10.1063/1.3449143]

I. INTRODUCTION

The nature of the molecular interactions that occur at interfaces is responsible for many of the phenomena that are observed in practice. For example, the formation of micelles by amphiphilic surfactant molecules in aqueous solutions (soap formulations and cosmetics), the nature of the lipid bilayers that form cell membranes, the stability of colloids in emulsions (such as milk and paint), etc. A detailed knowledge of interfacial properties is required to deal with many industrial processes, especially those related to separation and extraction. However, the modeling of interfacial systems remains a challenge precisely because of their inhomogeneous nature.

A quantitative evaluation of interfacial phenomena can be developed by starting from an accurate representation of the bulk homogeneous fluids. Among several possibilities, one of the most successful equations of state (EOSs) for fluid-phase equilibria is the statistical associating fluid theory (SAFT).[1,2] The general form of the SAFT expression for the Helmholtz free energy stems from the first-order perturbation theory for associating systems by Wertheim.[3–5] The total free free energy comprises a sum of terms that contribute to the total energy of the systems, each with a rigorous statistical mechanical foundation. Several versions of the SAFT approach have now been developed, most of them differing in the treatment of the reference term; among them, some of the most popular include SAFT-VR,[6,7] soft-SAFT,[8] PC-SAFT,[9] or the very recent SAFT-γ[10,11] incarnations of the methodology. Further details of the applicability and the various versions of SAFT can be found in the comprehensive reviews of Müller and Gubbins,[12] Economou,[13] Paricaud *et al.*,[14] and more recently, Tan *et al.*[15]

EOSs of the generic SAFT form can be used as a good basis for a specific treatment of the inhomogeneities of the density in the interfacial region. Moreover, the firm physical

a)Author to whom correspondence should be addressed. Electronic mail: g.jackson@imperial.ac.uk.

basis of the theory and the corresponding interpretation of the intermolecular interactions enables one to develop a methodology which can be used not only to predict but to understand the phenomena observed in real compounds.

A large body of literature has been devoted to the description and estimation of the interfacial properties of pure fluids following a variety of approaches. However, the application of theories of inhomogeneous systems to fluids mixtures is far less common. One of the first successful approaches for the description of interfacial tensions in mixtures is the so-called parachor method, introduced by Macleod.[16,17] One can use this empirical approach to correlate the interfacial tension with the difference of the bulk coexisting densities. Despite its empirical basis, Fowler[18] showed that the relation can be derived as an explicit function of the intermolecular potential in the case of a stepwise density profile, which is a reasonable assumption far away from the critical point. Other popular approaches are based on the corresponding-states principle of Guggenheim,[19] where empirical relations can be developed in terms of a specific reference fluid to provide an accurate representation of the surface tension.[20] Though useful in correlating data for the interfacial tension of fluid mixtures, these empirical relations offer little in way of predictive capability. This is the advantage of approaches developed from a more rigorous theoretical foundation such as the squared gradient theory [also referred to as density gradient theory (DGT)] and density functional theory (DFT).

The DGT methodology is rooted in the original theory for inhomogeneous fluids of van der Waals[21] (and in the earlier work by Rayleigh[22]), which was rediscovered and popularized by Cahn and Hilliard.[23] In DGT, the local free-energy density is expanded as a Taylor series about the density profile to second order, i.e., to the second derivative of the profile with respect to the distance from the interface (which in this case also corresponds to the square of the density gradient). The first term of the DGT essentially corresponds to the Helmholtz free-energy density of the uniform fluid evaluated at the local density. The square-gradient term can be expressed in terms of $c(r)$, the direct correlation function;[24] because the form of $c(r)$ is generally unknown, it is often treated phenomenologically with the help of an adjustable parameter, the so-called "influence" parameter, which is estimated from real surface tension data. This can limit the predictive capability of DGT approaches when extending the method to mixtures. We highlight some representative examples of studies where a DGT treatment has been employed in the following discussion. One of the first contributions in the area was the work of Carey *et al.*,[25,26] who used the Peng–Robinson (PR) cubic EOS within a DGT treatment to evaluate the interfacial properties for a wide variety of hydrocarbons, including alkanes, alkanols, and aromatics. At about the same time, Poser and Sanchez[27] combined a lattice theory with DGT to describe the interfacial tension of hydrocarbon mixtures and polymeric systems. Peters and collaborators have made extensive use of the density gradient approach with the PR EOS or with the associating-perturbed-anisotropic-chain theory (APACT) to study binary and ternary mixtures of carbon dioxide +butane+decane,[28,29] water+benzene,[30,31] water+ethanol +hexane,[31,32] and gas condensates of *n*-alkane mixtures.[33] Similar studies with other cubic EOSs have been made to describe the interfacial tension of a wide variety of mixtures including: light gases (carbon dioxide, nitrogen, or methane) and hydrocarbons;[34–36] refrigerants, nitrogen, argon, alkanes, and carbon dioxide;[37] and associating and nonassociating mixtures.[38,39] From a more formal perspective, Mejia and Segura[40,41] have studied the interfacial behavior of type IV binary mixtures (with regions of both vapor-liquid and liquid-liquid equilibria) by combining DGT with the van der Waals equation of state. This interesting analysis was then extended to the interfacial behavior exhibited by type I, type II, and type V binary mixtures of equal sized Lennard-Jones molecules using a more realistic DGT+soft-SAFT treatment,[42,43] including a comparison with molecular simulation. Kahl and Enders[44,45] were the first to combine a DGT treatment with the SAFT EOS to study the interfacial tension of mixtures of alkanes and of alkanes with methanol. In a series of subsequent studies, Enders and co-workers compared the performance of DGTs based on the PR, Sanchez–Lacombe (SL), SAFT, and PC-SAFT EOSs for mixtures of carbon dioxide and polystyrene,[46] associating mixtures of water and alkanols,[47] and mixtures of hydrocarbons and aromatics.[48] Numerous studies in which a SAFT-like description is used within a DGT formalism to describe the interfacial properties of fluid mixtures have now been made.[49–54]

One of the most successful and rigorous approaches for the description of inhomogeneous systems involves the formal application of DFT which, in contrast to DGT approaches, does not require the use of empirical adjustable parameters. DFT methods are based on the construction of a free-energy functional of the single particle density which fully describes the thermodynamic properties of the inhomogeneous system with an interface. Though the functional form of the free energy in typical DFTs is mathematically more complex (involving iterative variational techniques for their solution) than for a DGT treatment, they have become quite popular because of the enhanced predictive capability. As a consequence, intermolecular parameters which have been estimated by optimization of experimental data for the bulk phases are sufficient to provide a predictive platform for the interfacial properties of the system within a DFT formalism without the need for additional surface tension data. The fundamental details of the DFT approach can be found in the seminal reviews by Evans[55] and Davis,[56] including the various options for going from a general DFT formalism to an approximated theory that can be used to compute accurate results when applied to real fluids. For a recent overview of the numerous applications of DFT to pure fluids, the reader is referred to some of our previous publications[57–60] and to the recent work of Gross.[61]

As far as the application to real fluid mixtures is concerned, much fewer studies have been undertaken with DFT. One of the simplest free-energy functionals for the description of the interfacial properties of inhomogeneous mixtures involves a DFT constructed in a standard perturbative form: the repulsive reference term (which corresponds to the contribution from the hard-core interaction) is treated simply

with a local density approximation (LDA) using the free-energy density of the bulk reference fluid, and the perturbation term due to the attractive interactions is treated at the mean-field (MF) level assuming that one can neglect the correlations between the molecules. This type of approach is commonly referred to as a MF DFT.[62,63] Studies employing MF DFTs of this type have been used in a beautifully thorough series of studies by Telo da Gama and co-workers[64–79] to describe the vapor-liquid and liquid-liquid interfacial tension, the surface absorption, and the wetting behavior for a variety of mixtures of spherical particles. A quantitative assessment of the theory is then made by comparison with the interfacial data for mixtures of halocarbons. Nordholm and collaborators[80–82] have also developed a generalized van der Waals theory of interfaces, based on a perturbative DFT treated with a LDA, and have applied it to mixtures of alkanes and light gases. In an interesting and recent study, Bryk *et al.*[83] have employed DFT to study the phase behavior and the interfacial structure of two coexisting (liquid-vapor and liquid-liquid) phases and adsorption in slitlike pores for binary mixtures of chain and spherical particles. They used the same functional proposed by Yu and Wu.[84] The hard-sphere and chain terms (short-range part of the Helmholtz free-energy functional) are approximated with a weighted density approximation (WDA). In a WDA approach, one proposes a weighted (smoothed) density which depends on several weighting factors ω_i. The functions that define the different density weights are now often based on the fundamental measured theory of Rosenfeld[85] and its modifications.[86,87] This approximation accurately describes the oscillatory density profiles which are characteristic of fluid-solid interfaces (i.e., near a hard surface or for confined fluids, etc.). The attractive term is nonlocal and commonly evaluated at the MF level. Chapman and co-workers[88–91] have developed a general WDA-DFT approach based on Wertheim's first-order perturbation theory (iSAFT) to study the interfacial phenomena of polyatomic fluid mixtures including models of lipidlike molecules near surfaces, lipid bilayers, copolymer thin films, and diblock copolymers, though no direct comparison with experiment is made. Winkelmann and collaborators[92,93] have also used a DFT treatment to describe the interfacial properties of mixtures of Lennard-Jones molecules. The LDA and the WDA approaches were implemented to estimate the short-range contributions to the free-energy density. The attractive nonlocal term was calculated using a MF approximation. Moreover, they considered the capillary-wave "correction" by means of a mode-coupling theory for the mean-square roughness of the interface.[94] They applied the approach to calculate the vapor-liquid interface of the argon+methane, argon +nitrogen, heptane+toluene, and dimethyl formamide +heptane+toluene mixtures[92] and to evaluate the liquid-liquid interface of hypothetical binary and ternary mixtures.[93] More recently, Kahl and Winkelmann[95] have coupled the DFT treatment with the LJ-SAFT equation of state for molecules with segments interacting through the Lennard-Jones (LJ) interaction potential to predict surface tensions of a wide variety of pure nonassociating hydrocarbons. In this case, the radial distribution function in the attractive term is factorized out of the integral and written in terms of an effective contact value of the pair correlation function, as suggested by Gil-Villegas *et al.*[6] for the SAFT-VR approach which can be formulated as a DFT;[59,60] the accuracy of this approximation has been confirmed by comparison with the simulation data for vapor-liquid surface tension of square-well fluids of variable range.[96] Kahl and Winkelmann[95] also included a capillary-wave treatment which required the use of an empirical adjustable parameter, the value of which depended on the family of compounds; quantitative agreement was obtained in all cases when compared to experimental data.

In this paper, we address the problem of applying the DFT using a standard perturbative approach to study the interfacial properties of a range of fluid mixtures. We develop a generic DFT based on the SAFT-VR free energy,[6] which has been shown to provide an excellent predictive platform for the vapor-liquid and liquid-liquid equilibria of a range of systems (including alkanes and perfluoroalkanes,[97–100] replacement refrigerants,[101] water,[102,103] hydrogen chloride,[104] hydrogen fluoride,[105,106] carbon dioxide,[107,108] xenon,[109–113] boron trifluoride,[114] aqueous electrolytes,[115,116] and polyethylene[14,117–119] and polyoxyethylene polymers[120]) to treat the interfacial tension of inhomogeneous mixtures of associating and nonassociating chainlike molecules. Two approximate functionals are formulated and assessed in terms of their predictive capability for the interfacial tension of mixtures: the first involves the use of a MF attractive perturbative contribution with all of the short-range contributions (including those due to dispersion and hydrogen-bonding interactions) incorporated in a reference term which is treated locally; in the second, more rigorous approach, the correlations are retained in the attractive term by using average segment-segment correlation functions for the various components in the mixture evaluated at an average density across the density profile.

The rest of this article is organized as follows. In Sec. II, the theory is presented with the main details of the DFT approach. Particular attention is paid to the extension to mixtures and the description of the two approaches to approximate the contribution of the correlation function in the inhomogeneous region. In Sec. III, the new theory is used to study the influence of the molecular parameters on the interfacial phenomena for model binary mixtures. Both methodologies are then assessed for some representative mixtures of alkanes, comparing the predictions for the interfacial tension with experimental data. Finally, Sec. IV is devoted to the conclusions of this work.

II. THE DFT

In this work, we consider mixtures of chains of m_i spherical segments of diameter σ_{ii}, which can interact through pairwise repulsive, dispersive, and associative contributions. The repulsive and dispersive interactions characterizing each spherical segment are described by a simple square-well potential,

$$\phi_{ij}(r_{ij}) = \begin{cases} \infty & r_{ij} \leq \sigma_{ij} \\ -\epsilon_{ij} & \sigma_{ij} < r_{ij} \leq \lambda_{ij}\sigma_{ij} \\ 0 & r > \lambda_{ij}\sigma_{ij} \end{cases}, \quad (1)$$

where r_{ij} denotes the distance between the centers of the two segments, σ_{ij} defines the contact distance between segments of type i and j, and $\lambda_{ij}\sigma_{ij}$ denotes the range of the dispersive interaction of depth $-\epsilon_{ij}$.

The calculation of mixture properties requires the determination of a number of cross (unlike) intermolecular parameters. The Lorentz combining rule for mixtures is used for the unlike hard-core diameter,

$$\sigma_{ij} = \frac{\sigma_{ii} + \sigma_{jj}}{2}, \quad (2)$$

while in general, the unlike dispersive energy is given by the modified Berthelot combining rule for binary mixtures,

$$\epsilon_{ij} = (1 - k_{ij})\sqrt{\epsilon_{ii}\epsilon_{jj}}, \quad (3)$$

where k_{ij} quantifies the deviation from the Berthelot rule. In the particular case of the mixtures examined in this work, we employ the standard Berthelot recipe where $k_{ij}=0$. The unlike range parameter of the binary mixtures is obtained from the following relation:

$$\lambda_{ij} = \frac{\lambda_{ii}\sigma_{ii} + \lambda_{jj}\sigma_{jj}}{\sigma_{ii} + \sigma_{jj}}. \quad (4)$$

The association (hydrogen-bonding) contribution is modeled by considering additional off-center sites [placed a distance $r_d^{(i)}$ from the center of a given segment] which interact through a square-well potential of shorter range $r_c^{(ij)}$; the interaction of a site A on one segment with a site B on another is given by

$$\phi_{AB}^{ij}(r_{AB}^{(ij)}) = \begin{cases} -\epsilon_{AB}^{(ij)} & r_{AB}^{(ij)} < r_c^{(ij)} \\ 0 & r_{AB}^{(ij)} > r_c^{(ij)} \end{cases}, \quad (5)$$

where $r_{AB}^{(ij)}$ is the distance between the centers of the two associating sites A and B placed on segments of type i and j, respectively. In spite of its simplicity, this model includes the relevant features found in associating chain molecules: repulsive, attractive, and associative interactions.

A. Homogeneous fluid of associating chain molecules (SAFT-VR)

Within the SAFT-VR approach, the Helmholtz free energy A of the homogeneous fluid is written as a perturbation expansion which takes into account the various types of interactions. In the case of associating molecules, the free energy can be expressed as a sum of an ideal contribution A^{ideal}, a monomer term A^{mono} (which takes into account the attractive and repulsive forces between the segments that form the molecules), a chain contribution A^{chain} (which accounts for the connectivity of the segments in the molecules), and a contribution due to association A^{assoc}[6,7]

$$a = \frac{A}{Nk_BT} = \frac{A^{\text{ideal}}}{Nk_BT} + \frac{A^{\text{mono}}}{Nk_BT} + \frac{A^{\text{chain}}}{Nk_BT} + \frac{A^{\text{assoc}}}{Nk_BT}, \quad (6)$$

where N is the number of chain molecules in the mixture, T is the temperature, and k_B is the Boltzmann constant.

In the following, we use the nomenclature $a(\{\rho_m\}) \equiv a(\rho_1, \rho_2, \ldots, \rho_n)$ to denote the dependence of a or any other magnitude on all the densities ρ_m of each component m of the mixture. Here, m runs from 1 to n, with n the number of components of the mixture.

1. Ideal contribution

The ideal term is given in the standard form as[121]

$$a^{\text{ideal}}(\{\rho_m\}) \equiv \frac{A^{\text{ideal}}}{Nk_BT} = \sum_{i=1}^{n} x_i[\ln(\rho_i\Lambda_i^3) - 1], \quad (7)$$

where x_i is the mole fraction, $\rho_i = N_i/V$ is the number density of chain molecules of type i, N_i is the number of molecules, and Λ_i is a thermal de Broglie wavelength which contains the translational and rotational contributions to the partition function of the ideal chain corresponding to each component i of the mixture; the kinetic contributions do not have to be specified explicitly as they do not contribute to the fluid-phase equilibria and interfacial properties.

2. Monomer contribution

The term A^{mono} combines the repulsive and dispersive contributions to the free energy of the monomeric spherical segments making up the chain molecules. A high-temperature Barker and Henderson[122,123] perturbation expansion (truncated at second order) about a hard-sphere reference system is used to describe the free energy of the monomers:

$$a^{\text{mono}}(\{\rho_m\}) \equiv \frac{A^{\text{mono}}}{Nk_BT} = \left(\sum_{i=1}^{n} m_i x_i\right)(a^{\text{hs}} + a_1 + a_2). \quad (8)$$

The factor that depends on the chain length m_i and composition x_i of each component of the mixture appears in the expression because the monomer free energy is given in terms of the number of chain molecules N and not in terms of the number of monomer segments $N_s = (\Sigma_{i=1}^{n} x_i m_i)N$.

The reference hard-sphere term is obtained from the expression proposed independently by Boublík[124] and Mansoori *et al.*,[125]

$$a^{\text{hs}}(\{\rho_m\}) \equiv \frac{A^{\text{hs}}}{N_s k_B T} = \frac{6}{\pi\rho_s}\left[\left(\frac{\xi_2^3}{\xi_3^2} - \xi_0\right)\ln(1 - \xi_3) + \frac{3\xi_1\xi_2}{1 - \xi_3} + \frac{\xi_2^3}{\xi_3(1 - \xi_3)^2}\right], \quad (9)$$

where $\rho_s = N_s/V$ is the number density of spherical segments, which is related to ρ, the number density of chain molecules, through the relationship $\rho_s = \rho(\Sigma_{i=1}^{n} m_i x_i)$. ξ_k are the moment densities defined as

$$\xi_k = \frac{\pi}{6}\rho_s\left[\sum_{i=1}^{n} x_{si}(\sigma_{ii})^k\right], \tag{10}$$

where σ_{ii} is the diameter of the spherical segments of chain i and x_{si} is the mole fraction of segments of type i in the mixture which is given by

$$x_{si} = \frac{m_i x_i}{\Sigma_{k=1}^{n} m_k x_k}. \tag{11}$$

Note that the reduced packing fraction ξ_3 is the overall packing fraction of the mixture

$$\xi_3 = \frac{\pi}{6}\rho_s\sum_{i=1}^{n} x_{si}\sigma_{ii}^3 = \frac{\pi}{6}\sum_{i=1}^{n}\rho_{si}\sigma_{ii}^3 = \frac{\pi}{6}\sum_{i=1}^{n} m_i\sigma_{ii}^3\rho_i. \tag{12}$$

The last equation indicates that the overall packing fraction ξ_3 is a function of the densities of all of the components of the mixture $\xi_3 \equiv \xi_3(\{\rho_m\})$. Hence, all thermodynamic and structural properties that have an explicit dependence on ξ_3 are functions of the set of densities $\{\rho_m\}$. For clarity, in the rest of the section, we will indicate this dependency on the set of densities $\{\rho_m\}$.

In the context of the SAFT-VR approach for mixtures, the mean-attractive dispersive energy a_1 is described by[6,7]

$$a_1(\{\rho_m\}) \equiv \frac{A_1}{N_s k_B T} = \sum_{i=1}^{n}\sum_{j=1}^{n} x_{si}x_{sj}a_1^{(ij)}, \tag{13}$$

where $a_1^{(ij)}$ can be expressed with the use of the mean-value theorem as

$$a_1^{(ij)} = \frac{\rho_s}{k_B T}\sum_{i=1}^{n}\sum_{j=1}^{n} x_{si}x_{sj}\alpha_{ij}^{\mathrm{vdW}} g_0^{\mathrm{hs}}[\sigma_x;\xi_x^{\mathrm{eff}}(\lambda_{ij})], \tag{14}$$

where

$$\alpha_{ij}^{\mathrm{vdW}} = -\frac{2}{3}\pi\epsilon_{ij}\sigma_{ij}^3(\lambda_{ij}^3 - 1) \tag{15}$$

is the van der Waals attractive constant for the $i-j$ segment-segment interaction. $g_0^{\mathrm{hs}}[\sigma_x;\xi_x^{\mathrm{eff}}(\lambda_{ij})]$ is the contact value of the pair distribution function for the hard-sphere fluid at the effective density ξ_x^{eff}

$$g_0^{\mathrm{hs}}[\sigma_x;\xi_x^{\mathrm{eff}}(\lambda_{ij})] = \frac{1-\xi_x^{\mathrm{eff}}(\lambda_{ij})/2}{(1-\xi_x^{\mathrm{eff}}(\lambda_{ij}))^2}. \tag{16}$$

The dependence of $\xi_x^{\mathrm{eff}}(\lambda_{ij})$ on the packing fraction ξ_x and the range of the square-well potential λ_{ij} is obtained by using a very accurate description of the structure of the hard-sphere reference system with the following parametrization obtained for a square-well fluid:[6,7]

$$\xi_x^{\mathrm{eff}}(\lambda_{ij}) = c_1(\lambda_{ij})\xi_x + c_2(\lambda_{ij})\xi_x^2 + c_3(\lambda_{ij})\xi_x^3, \tag{17}$$

where the coefficients c_n are obtained from the matrix

$$\begin{pmatrix} c_1 \\ c_2 \\ c_3 \end{pmatrix} = \begin{pmatrix} 2.258\,55 & -1.053\,49 & 0.249\,434 \\ -0.692\,70 & 1.400\,49 & -0.827\,739 \\ 10.1576 & -15.0427 & 5.308\,27 \end{pmatrix}\begin{pmatrix} 1 \\ \lambda_{ij} \\ \lambda_{ij}^2 \end{pmatrix}. \tag{18}$$

Though the specific expressions presented here are for segment-segment interactions of a square-well form, the SAFT-VR treatment is entirely general[6] and has been implemented for Yukawa,[126] Lennard-Jones,[127] and Mie[128] potentials. The packing fraction ξ_x of the mixtures is defined in terms of σ_x, the segment size described in terms of a van der Waals one-fluid mixing rule:

$$\xi_x = \frac{\pi}{6}\rho_s\sigma_x^3 = \frac{\pi}{6}\rho_s\sum_{i=1}^{n}\sum_{j=1}^{n} x_{si}x_{sj}\sigma_{ij}^3. \tag{19}$$

As will become clear in Sec. II B 2, it is useful to partition the mean-attractive energy $a_1(\{\rho_m\}) = a_1^{\mathrm{sr}}(\{\rho_m\}) + a_1^{\mathrm{lr}}(\{\rho_m\})$ into short-range (a_1^{sr}) and long-range (a_1^{lr}) parts. The long-range contribution is simply the van der Waals dispersive term, which can be obtained from Eq. (14) fixing $g_0^{\mathrm{hs}} = 1$:

$$a_1^{\mathrm{lr}}(\{\rho_m\}) \equiv a_1(\{\rho_m\}; g_0 = 1) = \frac{\rho_s}{k_B T}\sum_{i=1}^{n}\sum_{j=1}^{n} x_{si}x_{sj}\alpha_{ij}^{\mathrm{vdW}}. \tag{20}$$

Note that this partitioning will provide a methodology for the generalization of the original SAFT-VR DFT treatment[59,60] to mixtures; we emphasize that this does not mean that our current description involves a MF approximation of the type employed in the less rigorous augmented van der Waals approaches (e.g., see Refs. 129–134, which include studies with EOSs of the SAFT form). The short-range contribution can be obtained simply by subtracting this long-range contribution from the total free energy, $a_1^{\mathrm{sr}}(\{\rho_m\}) = a_1(\{\rho_m\}) - a_1^{\mathrm{lr}}(\{\rho_m\})$,

$$a_1^{\mathrm{sr}}(\{\rho_m\}) = \frac{\rho_s}{k_B T}\sum_{i=1}^{n}\sum_{j=1}^{n} x_{si}x_{sj}\alpha_{ij}^{\mathrm{vdW}}\{g_0^{\mathrm{hs}}[\sigma_x;\xi_x^{\mathrm{eff}}(\lambda_{ij})] - 1\}, \tag{21}$$

where $h_0^{\mathrm{hs}}[\sigma_x;\xi_x^{\mathrm{eff}}(\lambda_{ij})] = g_0^{\mathrm{hs}}[\sigma_x;\xi_x^{\mathrm{eff}}(\lambda_{ij})] - 1$ is an effective total correlation function. The second-order perturbation (fluctuation) term is expressed in terms of the local compressibility approximation (LCA) proposed by Barker and Henderson,[135] where the fluctuation of the attractive energy is related directly to the compressibility of the system by

$$a_2(\{\rho_m\}) \equiv \frac{A_2}{N_s k_B T} = \sum_{i=1}^{n}\sum_{j=1}^{n}\frac{1}{2}\left(\frac{\epsilon_{ij}}{k_B T}\right)K^{\mathrm{hs}} x_{si}x_{sj}\rho_s\frac{\partial a_1^{(ij)}}{\partial\rho_s}. \tag{22}$$

Here, K^{hs} is the isothermal compressibility for a mixture of hard spheres, given by the Percus–Yevick expression[136]

$$K^{\mathrm{hs}} = \frac{\xi_0(1-\xi_3)^4}{\xi_0(1-\xi_3)^2 + 6\xi_1\xi_2(1-\xi_3) + 9\xi_2^3}. \tag{23}$$

3. Chain contribution

The contribution to the free energy due to the formation of a mixture of chain molecules from the atomized segments is given in the standard Wertheim TPT1 form as[137]

$$a^{\text{chain}}(\{\rho_m\}) \equiv \frac{A^{\text{chain}}}{Nk_BT} = -\sum_{i=1}^{n}(m_i - 1)\ln g_{ii}^{\text{sw}}(\sigma_{ii};\{\rho_m\}), \tag{24}$$

where $g_{ii}^{\text{sw}}(\sigma_{ii};\{\rho_m\})$ is the contact value of the pair correlation function for a system of square-well monomers. In the SAFT-VR approach, the contact value of the pair radial distribution function $g_{ii}^{\text{sw}}(\sigma_{ii};\{\rho_m\})$ is obtained from a first-order high-temperature expansion about a hard-sphere reference system[6,7]

$$g_{ij}^{\text{sw}}(\sigma_{ij};\{\rho_m\}) = g_{ij}^{\text{hs}}(\sigma_{ij};\{\rho_m\}) + \beta\epsilon_{ij}g_1^{(ij)}(\sigma_{ij};\{\rho_m\}), \tag{25}$$

where g_{ij}^{hs} is the contact value of the radial distribution function for the reference system of a mixture of hard spheres at the packing fraction ξ_3 of the mixture:

$$g_{ij}^{\text{hs}}(\sigma_{ij};\xi_3) = \frac{1}{1-\xi_3} + 3D_{ij}\frac{\xi_3}{(1-\xi_3)^2} + 2D_{ij}^2\frac{\xi_3^2}{(1-\xi_3)^3}, \tag{26}$$

where D_{ij} is defined as

$$D_{ij} = \frac{\sigma_{ii}\sigma_{jj}}{\sigma_{ii}+\sigma_{jj}}\frac{\Sigma_{k=1}^{n}x_{sk}\sigma_{kk}^2}{\Sigma_{k=1}^{n}x_{sk}\sigma_{kk}^3}. \tag{27}$$

The term $g_1^{(ij)}(\sigma_{ij};\{\rho_m\})$ is obtained from a self-consistent calculation of the pressure using the Claussius virial theorem, as explained in the original SAFT-VR paper.[6,7] For a mixture of square-well monomers, $g_1^{(ij)}$ is given by

$$g_1^{(ij)}(\sigma_{ij};\{\rho_m\}) = \frac{1}{2\pi\epsilon_{ij}\sigma_{ij}^3}\left[3\left(\frac{\partial a_i^{(ij)}}{\partial\rho_s}\right) - \frac{\lambda_{ij}}{\rho_s}\frac{\partial a_i^{(ij)}}{\partial\lambda_{ij}}\right]. \tag{28}$$

4. Association contribution

The association contribution to the free energy, which is at the heart of all SAFT EOSs, is described with the Wertheim[3–5] theory of association. This term can be expressed as a function of the fraction of molecules not bonded at given sites as[138]

$$a^{\text{assoc}}(\{\rho_m\}) \equiv \frac{A^{\text{assoc}}}{Nk_BT} = \sum_{i=1}^{n}x_i\left[\left\{\sum_{A=1}^{s_i}\left(\ln X_A^{(i)} - \frac{X_A^{(i)}}{2}\right) + \frac{1}{2}\right\}\right], \tag{29}$$

where the first sum is over the species i and the second is over all s_i sites A on a molecule of species i. $X_A^{(i)}$ is the fraction of molecules of type i not bonded at a given site A, given by the mass-action equation as

$$X_A^{(i)} = \frac{1}{1+\Sigma_{j=1}^{n}\Sigma_{B=1}^{s_j}\rho_j X_B^{(j)}\Delta_{AB}^{(ij)}}, \tag{30}$$

where B denotes the set of sites capable of bonding with site A. The association interaction parameter $\Delta_{AB}^{(ij)}$ is determined from the Mayer function $F_{AB}^{(ij)} = [\exp(\epsilon_{AB}^{(ij)}/k_BT) - 1]$, the volume $K_{AB}^{(ij)}$ available for bonding between sites A and B, and the contact value of the monomer pair radial distribution function as[138]

$$\Delta_{AB}^{(ij)} = F_{AB}^{(ij)}K_{AB}^{(ij)}g_{ij}^{\text{sw}}(\sigma_{ij};\{\rho_m\}). \tag{31}$$

The free energy that has been described for the homogeneous fluid of associating chain molecules can be used to determine the bulk vapor-liquid equilibria in a straightforward fashion. The densities of the coexisting vapor and liquid states at a fixed temperature and pressure are determined numerically by requiring that the pressure $P = -(\partial A/\partial V)_{T,N}$ and chemical potentials $\mu_i = -(\partial A/\partial N_i)_{T,V,N_{j\neq i}}$ of each component i in the two phases are equal.

Now that the contributions to the free energy of the bulk fluid of associating chain molecules have been defined, we can construct the perturbative free-energy functional for the inhomogeneous fluid.

B. Inhomogeneous fluid of associating chain molecules (SAFT-VR DFT)

We consider an open mixture at temperature T and chemical potential μ_i for each component in a volume V. In the absence of external fields, the grand potential functional $\Omega[\{\rho_m(\mathbf{r})\}]$ of an inhomogeneous system is given by[55]

$$\Omega[\{\rho_m(\mathbf{r})\}] = A[\{\rho_m(\mathbf{r})\}] - \sum_{i=1}^{n}\mu_i\int d\mathbf{r}\rho_i(\mathbf{r}), \tag{32}$$

where $A[\{\rho_m(\mathbf{r})\}]$ is the "intrinsic" Helmholtz free-energy functional. As in the case of homogeneous systems, we use the nomenclature $A[\{\rho_m(\mathbf{r})\}] \equiv A[\rho_1(\mathbf{r}),\rho_2(\mathbf{r}),\ldots,\rho_n(\mathbf{r})]$ to denote the functional dependence of A on all of the densities $\rho_m(\mathbf{r})$ (at each point $\mathbf{r}$) for the set of components m of the mixture. In general, the notation $\{\rho_m(\mathbf{r})\}$ is used to denote all the density profiles of the mixture evaluated at position $\mathbf{r}$, i.e., $\{\rho_m(\mathbf{r})\} \equiv \rho_1(\mathbf{r}),\rho_2(\mathbf{r}),\ldots,\rho_n(\mathbf{r})$. The minimum value of $\Omega[\{\rho_m(\mathbf{r})\}]$ is the equilibrium grand potential of the system and the corresponding equilibrium density profiles $\rho_i^{\text{eq}}(\mathbf{r})$ satisfy the following condition:[55]

$$\left.\frac{\delta\Omega[\{\rho_m(\mathbf{r})\}]}{\delta\rho_i(\mathbf{r})}\right|_{\text{eq}} = \left.\frac{\delta A[\{\rho_m(\mathbf{r})\}]}{\delta\rho_i(\mathbf{r})}\right|_{\text{eq}} - \mu_i = 0 \quad \forall \quad i = 1\ldots n. \tag{33}$$

These n Euler–Lagrange equations are equivalent to requiring that the Helmholtz free-energy functional be a minimum subject to a constraint of constant number of particles; the undetermined multipliers correspond to the chemical potentials of each component μ_i in the bulk coexisting phases.

In this work, we extend the previous SAFT-VR DFT formalism[59,60] to mixtures of associating chain molecules. As for pure fluids, we follow a standard perturbative approach[55,92] where the intermolecular potential is partitioned into a reference term (which includes the ideal, hard-sphere, chain, and short-range association contributions) and a perturbation attractive term (which includes the dispersive interactions between the monomeric segments). Here we consider two different levels of approximation to account for the description of the fluid interface. In the first approach

(SAFT-VR DFT), both the bulk fluid-phase equilibria and the interfacial properties are described with a perturbation theory in which correlations are included in the reference and dispersive terms. In the second approximate scheme (SAFT-VR MF DFT), the bulk fluid is treated at the SAFT-VR level (a second-order perturbation theory which incorporates the correlations of the hard-sphere reference system), while the interfacial properties are treated at the MF level (the correlations are neglected in the dispersive term).

1. SAFT-VR DFT

The Helmholtz free-energy functional in the full SAFT-VR treatment of a mixture of associating chain molecules describes both the bulk vapor-liquid equilibria and the interfacial properties within a perturbative approach. Correlations are taken into account explicitly both in the reference and dispersive terms. The full SAFT-VR free-energy functional is given by

$$A[\{\rho_i(\mathbf{r})\}] = A^{\text{ref}}[\{\rho_i(\mathbf{r})\}] + A^{\text{att}}[\{\rho_i(\mathbf{r})\}]. \tag{34}$$

It is convenient to examine the grand potential functional in terms of reduced free-energy densities $f[\rho(\mathbf{r})] \equiv A[\{\rho_m(\mathbf{r})\}]/Vk_BT \equiv (\Sigma_{i=1}^{n}\rho_i(\mathbf{r}))a[\{\rho_m(\mathbf{r})\}]$, where $a[\{\rho_m(\mathbf{r})\}] \equiv A[\{\rho_m(\mathbf{r})\}]/(Nk_BT)$.

As in our previous works,[57–60] the reference term A^{ref} is taken to incorporate all of the contributions to the free energy due to "short-range" interactions such as the repulsive hard-sphere term, the chain term, and the association term

$$\begin{aligned} A^{\text{ref}}[\{\rho_m(\mathbf{r})\}] = {} & A^{\text{ideal}}[\{\rho_m(\mathbf{r})\}] + A^{\text{hs}}[\{\rho_m(\mathbf{r})\}] \\ & + A_2[\{\rho_m(\mathbf{r})\}] + A^{\text{chain}}[\{\rho_m(\mathbf{r})\}] \\ & + A^{\text{assoc}}[\{\rho_m(\mathbf{r})\}]. \end{aligned} \tag{35}$$

The reduced ideal Helmholtz free energy of an inhomogeneous mixture of nonspherical particles can be written as[55,139]

$$A^{\text{ideal}}[\{\rho_m(\mathbf{r})\}] = \sum_{i=1}^{n} k_BT \int \mathrm{d}\mathbf{r}\rho_i(\mathbf{r})[\ln(\rho_i(\mathbf{r})\Lambda_i^3) - 1], \tag{36}$$

where the orientational coordinates have been integrated out to give a constant contribution as the phase is assumed to be isotropic.

The hard-sphere interaction is short ranged and is usually treated locally in a perturbative DFT treatment of the fluid interface;[55,92] such functionals based on the LDA of the reference term provide a good description of the vapor-liquid and liquid-liquid interfaces, although the approach fails for fluids close to their triple points or for confined systems where a WDA has to be used. In our SAFT-VR DFT the hard-sphere LDA free-energy functional is given by

$$\begin{aligned} A^{\text{hs}}[\{\rho_m(\mathbf{r})\}] &= k_BT \int \mathrm{d}\mathbf{r} f^{\text{hs}}(\{\rho_m(\mathbf{r})\}) \\ &= k_BT \int \mathrm{d}\mathbf{r} \left(\sum_{i=1}^{n} m_i\rho_i(\mathbf{r}) \right) a^{\text{hs}}(\{\rho_m(\mathbf{r})\}), \end{aligned} \tag{37}$$

where the expression for $a^{\text{hs}}(\{\rho_m(\mathbf{r})\})$ is written as a function of the packing fractions ξ_k defined in Eq. (10) from the Boublík and Mansoori *et al.* form [cf. Eq. (9)].

In the SAFT-VR description of the thermodynamics of the fluid, the high-temperature perturbation expansion of the free energy is taken to second order (A_2). The LCA is used to approximate the fluctuation term A_2 of the homogeneous system in terms of the compressibility of the hard-sphere fluid. This contribution is also treated locally in our reference term

$$\begin{aligned} A_2[\{\rho_m(\mathbf{r})\}] &= k_BT \int \mathrm{d}\mathbf{r} f_2(\{\rho_m(\mathbf{r})\}) \\ &= k_BT \int \mathrm{d}\mathbf{r} \left(\sum_{i=1}^{n} m_i\rho_i(\mathbf{r}) \right) a_2(\{\rho_m(\mathbf{r})\}), \end{aligned} \tag{38}$$

where $a_2(\{\rho_m(\mathbf{r})\})$ is given by Eq. (22). The slope of the profile for the mean-attractive energy turns out to be fairly constant over the interfacial region,[59] which suggests that the fluctuation term is reasonably constant and can be treated locally at a first level of approximation, since $\partial a_1(\{\rho_m(\mathbf{r})\})/\partial\rho_i \propto a_2(\{\rho_m(\mathbf{r})\})$. At this stage, we should point out that the second-order term has to be included in the full free-energy functional of the inhomogeneous system in order to recover the SAFT-VR expressions of the homogeneous bulk phase. This term was not taken into account in the earlier MF description of the SAFT-DFT approach.[57,58]

Both the hard-chain [cf. Eq. (9)] and the association [cf. Eq. (29)] contributions to the SAFT free energy can be written in terms of the contact value of the pair radial distribution function of the reference monomer system; this is clearly a short-range contribution and can also be approximated by a local functional. The contribution to the reference free-energy functional for the formation of chains of m_i square-well segments is written at the LDA level as

$$\begin{aligned} A^{\text{chain}}[\{\rho_m(\mathbf{r})\}] &= k_BT \int \mathrm{d}\mathbf{r} f^{\text{chain}}(\{\rho_m(\mathbf{r})\}) \\ &= k_BT \int \mathrm{d}\mathbf{r} \left(\sum_{i=1}^{n} m_i\rho_i(\mathbf{r}) \right) a^{\text{chain}}(\{\rho_m(\mathbf{r})\}), \end{aligned} \tag{39}$$

where $a^{\text{chain}}(\{\rho_m(\mathbf{r})\})$ is the function of density given by Eq. (24). The LDA treatment of long chains may at first appear to be rather drastic. As will be shown later, it nonetheless provides a good description of the vapor-liquid surface tension of moderately long alkanes. In essence, this approximation amounts to determining the average density profile for the segments making up the chain without specifying which chain the segments belong to. A more sophisticated WDA treatment, such as that developed by Kierlik and co-workers[140–142] in which the position of each segment of the chain is treated explicitly, can be used to improve the description of long chains. This is, however, beyond the scope of the current work.

In a similar way, we can write the contribution due to molecular association at the LDA level as

$$A^{\text{assoc}}[\{\rho_m(\mathbf{r})\}] = k_B T \int d\mathbf{r} f^{\text{assoc}}(\{\rho_m(\mathbf{r})\}) = k_B T \int d\mathbf{r} \left(\sum_{i=1}^{n} m_i \rho_i(\mathbf{r}) \right) a^{\text{assoc}}(\{\rho_m(\mathbf{r})\}), \tag{40}$$

where $a^{\text{assoc}}(\{\rho_m(\mathbf{r})\})$ is given by Eq. (29). The perturbation theory of Wertheim[3–5] was originally developed in the general case of inhomogeneous systems; the fraction $X_{\text{A}}^{(i)}[\{\rho_m(\mathbf{r})\}]$ of molecules of type i not bonded at a given site A at a point $\mathbf{r}$ in the fluid can be expressed as a set of mass-action equations:

$$X_{\text{A}}^{(i)}[\{\rho_m(\mathbf{r})\}] = \left[1 + \sum_{j=1}^{n} \sum_{\text{B}=1}^{s_j} \int d\mathbf{r}' d\omega' \rho_j(\mathbf{r}') X_{\text{B}}^{(j)}[\{\rho_m(\mathbf{r}')\}] \times F_{\text{AB}}^{(ij)} g_{ij}^{(\text{sw})}[\mathbf{r}, \mathbf{r}'; \{\rho_m(\mathbf{r}), \rho_l(\mathbf{r}')\}] \right]^{-1}. \tag{41}$$

We use the nomenclature $\{\rho_m(\mathbf{r}), \rho_l(\mathbf{r}')\}$ to denote a dependence with the density profiles evaluated at positions $\mathbf{r}$ and $\mathbf{r}'$, respectively. More explicitly, $\{\rho_m(\mathbf{r}), \rho_l(\mathbf{r}')\} \equiv \rho_1(\mathbf{r}), \rho_1(\mathbf{r}'), \rho_2(\mathbf{r}), \rho_2(\mathbf{r}'), \ldots, \rho_n(\mathbf{r})\rho_n(\mathbf{r}')$.

The mass-action equations are seen to be nonlocal in nature, i.e., the property at a point $\mathbf{r}$ depends on an integral over neighboring points $\mathbf{r}'$. The integral over orientations ω' for the site-site association interaction is also undertaken. In our local LDA treatment, we assume that the density does not vary appreciably over the range of the site-site association interaction, $\rho_i(\mathbf{r}') \approx \rho_i(\mathbf{r})$; this is expected to be a good approximation for hydrogen-bonding association where the range of the interaction is very short. The LDA form of the set of mass-action equations defined by Eq. (30) can thus be written as

$$X_{\text{A}}^{(i)}(\{\rho_m(\mathbf{r})\}) = \left[1 + \sum_{j=1}^{n} \sum_{\text{B}=1}^{s_j} \rho_j(\mathbf{r}) X_{\text{B}}^{(j)}(\{\rho_m(\mathbf{r})\}) \times \Delta_{\text{AB}}(\{\rho_m(\mathbf{r})\}) \right]^{-1}. \tag{42}$$

The correlations are included in the term $\Delta_{\text{AB}}^{(ij)}$ where we have invoked the additional approximation that $r^2 g_{ij}^{\text{sw}}[r; \{\rho_i(\mathbf{r})\}]$ does not vary appreciably over the range of the site-site interaction:[138]

$$\Delta_{\text{AB}}^{(ij)}(\{\rho_m(\mathbf{r})\}) = K_{\text{AB}}^{(ij)} F_{\text{AB}}^{(ij)} g_{ij}^{\text{sw}}(\sigma_{ij}; \{\rho_m(\mathbf{r})\}). \tag{43}$$

Before we end our description of the reference free-energy functional, it is instructive to note that within the LDA treatment, the free-energy density $f^{\text{ref}}(\{\rho_m(\mathbf{r})\})$ is thus as a simple function, not a functional, of the local density, which is represented by that of the homogeneous system.

Since we are dealing with chainlike molecules, the dispersive contribution can be expressed in terms of the average segment density profiles and the average segment-segment pair radial distribution function of the inhomogeneous reference hard-sphere chain. Following our previous work, we approximate the segment-segment pair distribution function by that of the equivalent unbonded hard-sphere mixture and express the functional in terms of the molecular density profiles as

$$A^{\text{att}}[\{\rho_m(\mathbf{r})\}] = \frac{1}{2} \sum_{i=1}^{n} \sum_{j=1}^{n} \int d\mathbf{r} m_i \rho_i(\mathbf{r}) \int d\mathbf{r}' m_j \rho_j(\mathbf{r}') \times g_{ij}^{\text{hs}}[\mathbf{r}, \mathbf{r}'; \{\rho_m(\mathbf{r}), \rho_l(\mathbf{r}')\}] \phi_{ij}^{\text{att}}(|\mathbf{r} - \mathbf{r}'|), \tag{44}$$

where we have expressed the functional in terms of the molecular densities profiles. Note that A^{att} depends on the set $\{\rho_m(\mathbf{r})\}$, i.e., on all of the density profiles of the mixture, but g_{ij}^{hs} also depends on $\{\rho_m(\mathbf{r}), \rho_l(\mathbf{r}')\}$, which means that the distribution function depends, in general, on all the density profiles of the mixture at $\mathbf{r}$ but also at $\mathbf{r}'$.

A further set of approximations are now required as little is known about the pair distribution function of the inhomogeneous hard-sphere fluid mixture.

(i) In order to extend the original SAFT-VR DFT formalism, originally developed for pure component systems, we use a simple van der Waals one-fluid approximation and define the local packing fractions at $\mathbf{r}$ and $\mathbf{r}'$ for the mixture as

$$\xi_x(\mathbf{r}) \equiv \xi_x(\{\rho_m(\mathbf{r})\}) = \frac{\pi}{6} \rho_s(\mathbf{r}) \sigma_x^3(\mathbf{r}) \equiv \frac{\pi}{6} \sum_{i=1}^{n} \sum_{j=1}^{n} \frac{m_i \rho_i(\mathbf{r}) m_j \rho_j(\mathbf{r})}{\rho_s(\mathbf{r})} \sigma_{ij}^3. \tag{45}$$

Note that the local packing fraction is a function of $\mathbf{r}$ through the set of all the density profiles of the mixture evaluated at $\mathbf{r}$. $\xi_x(\mathbf{r}')$ can be obtained from the same expression [Eq. (45)] simply by substitution of $\mathbf{r}$ by $\mathbf{r}'$. The total density of segments $\rho_s(\mathbf{r})$ is defined as

$$\rho_s(\mathbf{r}) \equiv \rho_s(\{\rho_m(\mathbf{r})\}) = \sum_{k=1}^{n} m_k \rho_k(\mathbf{r}), \tag{46}$$

and $\rho_s(\mathbf{r}')$ is again obtained by interchanging $\mathbf{r}$ by $\mathbf{r}'$. Note that Eq. (45) is the traditional van der Waals one-fluid mixing rule defined locally (at $\mathbf{r}$ and $\mathbf{r}'$), but expressed in terms of the molecular densities of the chains (instead of segment densities).

(ii) Following our previous work, we assume that the correlations can be described with the pair radial distribution function of an effective homogeneous fluid of (equivalent) hard spheres evaluated at an appropriate mean density. This procedure for evaluating the correlation function of the inhomogeneous system in terms of that for the homogeneous system at a mean density dates back to the work of Toxvaerd.[143–145] In this case, the mean packing fraction is calculated from the simple arithmetic average,

$$\overline{\xi}_x(\mathbf{r},\mathbf{r}') \equiv \overline{\xi}_x(\{\rho_i(\mathbf{r}),\rho_j(\mathbf{r}')\}) = \frac{\xi_x(\mathbf{r})+\xi_x(\mathbf{r}')}{2}, \tag{47}$$

where $\xi_x(\mathbf{r})$ and $\xi_x(\mathbf{r}')$ are the (true) inhomogeneous packing fraction at $\mathbf{r}$ and $\mathbf{r}'$, respectively. Note that $\overline{\xi}_x$ is a function of $\mathbf{r}$ and $\mathbf{r}'$ through the set of density profiles of the mixture evaluated at $\mathbf{r}$ and $\mathbf{r}'$.

(iii) A further approximation is required in order to have a closed set of equations. In line with the SAFT-VR treatment of the bulk fluid mixtures, $g_{ij}^{\mathrm{hs}}[\mathbf{r},\mathbf{r}';\{\rho_m(\mathbf{r}),\rho_l(\mathbf{r}')\}]$ can be approximated by a pair radial distribution function at contact for an equivalent one-component system with an effective packing fraction $\overline{\xi}_x^{\mathrm{eff}}(\lambda_{ij})$, which also depends on the set of densities $\{\rho_m(\mathbf{r}),\rho_l(\mathbf{r}')\}$. This inhomogeneous effective packing fraction can be obtained using the bulk expression [Eq. (17)], but evaluating all of the densities from the corresponding mean packing fraction determined for the set of density profiles at each pair of positions:

$$\begin{aligned}\overline{\xi}_x^{\mathrm{eff}}(\lambda_{ij};\{\rho_m(\mathbf{r}),\rho_l(\mathbf{r}')\}) &= c_1(\lambda_{ij})\overline{\xi}_x(\mathbf{r},\mathbf{r}') + c_2(\lambda_{ij})\overline{\xi}_x^2(\mathbf{r},\mathbf{r}') \\ &\quad + c_3(\lambda_{ij})\overline{\xi}_x^3(\mathbf{r},\mathbf{r}').\end{aligned} \tag{48}$$

In order to be consistent with our previous SAFT-VR functional in the homogeneous limit,[59,60] we use the following approximation:

$$g_{ij}^{\mathrm{hs}}[\mathbf{r},\mathbf{r}';\{\rho_m(\mathbf{r}),\rho_l(\mathbf{r}')\}] \approx g_0^{\mathrm{hs}}[\sigma_x;\overline{\xi}_x^{\mathrm{eff}}(\lambda_{ij};\{\rho_m(\mathbf{r}),\rho_l(\mathbf{r}')\})]. \tag{49}$$

The final expression for the attractive perturbation term used in the SAFT-VR DFT approach for mixtures is given by

$$\begin{aligned}A^{\mathrm{att}}[\{\rho_m(\mathbf{r})\}] = \frac{1}{2}\sum_{i=1}^{n}\sum_{j=1}^{n}\int \mathrm{d}\mathbf{r} m_i\rho_i(\mathbf{r})\int \mathrm{d}\mathbf{r}' m_j\rho_j(\mathbf{r}') \\ \times g_0^{\mathrm{hs}}[\sigma_x;\overline{\xi}_x^{\mathrm{eff}}(\lambda_{ij};\{\rho_m(\mathbf{r}),\rho_l(\mathbf{r}')\})]\phi_{ij}^{\mathrm{att}}(|\mathbf{r}-\mathbf{r}'|).\end{aligned} \tag{50}$$

As we mentioned earlier, the equilibrium interfacial profiles are those that minimize the grand potential. In the case of the SAFT-VR DFT that has just been described, the corresponding Euler–Lagrange equations are obtained as

$$\begin{aligned}\left.\frac{\delta\Omega[\{\rho_m(\mathbf{r})\}]}{\delta\rho_i(\mathbf{r})}\right|_{\mathrm{eq}} &= \left.\frac{\delta A[\{\rho_m(\mathbf{r})\}]}{\delta\rho_i(\mathbf{r})}\right|_{\mathrm{eq}} - \mu_i \\ &= \frac{\delta A^{\mathrm{ref}}[\{\rho_m(\mathbf{r})\}]}{\delta\rho_i(\mathbf{r})} + \frac{\delta A^{\mathrm{attr}}[\{\rho_m(\mathbf{r})\}]}{\delta\rho_i(\mathbf{r})} - \mu_i \\ &= 0 \quad \forall \ i = 1\ldots n.\end{aligned} \tag{51}$$

The variation of the reference contribution with respect to densities $\{\rho_i(\mathbf{r})\}$ correspond to the local chemical potential

$$\mu_i^{\mathrm{ref}} = \frac{\delta A^{\mathrm{ref}}[\{\rho_m(\mathbf{r})\}]}{\delta\rho_i(\mathbf{r})}, \tag{52}$$

which can be obtained from the corresponding expressions for the homogeneous system, through the thermodynamic identity:

$$\mu_i = k_BT\left\{a + \rho\left(\frac{\partial a}{\partial\rho_i}\right)_{TVN_{j\neq i}}\right\}. \tag{53}$$

However, the variation of the attractive contribution requires knowledge of the density derivative of the correlation function with respect to $\rho_i(\mathbf{r})$ [see Eq. (50)]. The equilibrium density profiles can thus be determined by solving the following equations:

$$\begin{aligned}\mu_i = \mu_i^{\mathrm{ref}}(\{\rho_m(\mathbf{r})\}) + \sum_{j=1}^{n}\int \mathrm{d}\mathbf{r}' m_i m_j\rho_j(\mathbf{r}') \\ \times g_0^{\mathrm{hs}}[\sigma_x;\overline{\xi}_x^{\mathrm{eff}}(\lambda_{ij};\{\rho_l(\mathbf{r}),\rho_m(\mathbf{r}')\})]\phi_{ij}^{\mathrm{attr}}(|\mathbf{r}-\mathbf{r}'|) \\ + \sum_{j=1}^{n}\sum_{k=1}^{n}\int \mathrm{d}\mathbf{r}' m_j\rho_j(\mathbf{r}) m_k\rho_k(\mathbf{r}') \\ \times \frac{\partial g_0^{\mathrm{hs}}[\sigma_x;\overline{\xi}_x^{\mathrm{eff}}(\lambda_{ij};\{\rho_l(\mathbf{r}),\rho_m(\mathbf{r}')\})]}{\partial\rho_i(\mathbf{r})}\phi_{ij}^{\mathrm{attr}}(|\mathbf{r}-\mathbf{r}'|).\end{aligned} \tag{54}$$

The relation ensures that the (local) chemical potential of each component i at each point along the profiles is equal to corresponding bulk chemical potential μ_i^{bulk}.

2. SAFT-VR MF DFT

It is convenient to have a general approach for the development of an accurate free-energy functional where one does not have to treat the correlations in the perturbative attractive term; this would allow one to construct a DFT from any engineering equation of state of the bulk fluid mixture which is not explicitly cast in terms of the correlation functions between the particles. In this section, we develop such an approach within the SAFT-VR description of homogeneous fluid mixtures, though the method is not restricted to SAFT-like EOSs. One can define a free-energy functional in which the bulk fluid is treated at the full SAFT-VR level (a second-order perturbation theory which incorporates the correlations of the hard-sphere reference system) and the interface is treated at the MF level of van der Waals (the correlations are neglected in the attractive term).

As in Sec. II B 1 the Helmholtz free-energy functional is expressed in terms of an ideal, a reference, and an attractive contribution [cf. Eq. (34)]:

$$A_{\mathrm{mf}}[\{\rho_m(\mathbf{r})\}] = A_{\mathrm{mf}}^{\mathrm{ref}}[\{\rho_m(\mathbf{r})\}] + A_{\mathrm{mf}}^{\mathrm{att}}[\{\rho_m(\mathbf{r})\}]. \tag{55}$$

The reference term $A_{\mathrm{mf}}^{\mathrm{ref}}[\{\rho_m(\mathbf{r})\}]$ is again treated locally, but is now defined as

$$\begin{aligned}A_{\mathrm{mf}}^{\mathrm{ref}}[\{\rho_m(\mathbf{r})\}] = A^{\mathrm{hs}}[\{\rho_m(\mathbf{r})\}] + A^{\mathrm{chain}}[\{\rho_m(\mathbf{r})\}] \\ + A_2[\{\rho_m(\mathbf{r})\}] + A_1^{\mathrm{sr}}[\{\rho_m(\mathbf{r})\}] \\ + A^{\mathrm{assoc}}[\{\rho_m(\mathbf{r})\}],\end{aligned} \tag{56}$$

where the full expressions for $A^{\text{hs}}[\{\rho_m(\mathbf{r})\}]$ [Eq. (37)], $A_2[\{\rho_m(\mathbf{r})\}]$ [Eq. (38)], $A^{\text{chain}}[\{\rho_m(\mathbf{r})\}]$ [Eq. (39)], and $A^{\text{assoc}}[\{\rho_m(\mathbf{r})\}]$ [Eq. (40)] are used. The contribution due to the short-range part of the correlations in the attractive term is contained in $A_1^{\text{sr}}[\{\rho_m(\mathbf{r})\}]$, which is defined in terms of the bulk term a_1^{sr} [Eq. (21)]. As this represents a relatively short-range interaction, it can be treated locally as

$$A_1^{\text{sr}}[\{\rho_m(\mathbf{r})\}] = k_B T \int d\mathbf{r} f_1^{\text{sr}}(\{\rho_m(\mathbf{r})\}) = k_B T \int d\mathbf{r} \left(\sum_{i=1}^{n} m_i \rho_i(\mathbf{r}) \right) a_1^{\text{sr}}(\{\rho_m(\mathbf{r})\}). \quad (57)$$

The MF dispersive term $A_{\text{mf}}^{\text{att}}[\{\rho_m(\mathbf{r})\}]$ is described at the level of the van der Waals MF approximation in which the correlations in the attractive perturbation term are neglected. By making the approximation $g_{ij}^{\text{hs}}[\mathbf{r},\mathbf{r}';\{\rho_m(\mathbf{r}),\rho_l(\mathbf{r}')\}] \approx 1$ in Eq. (44) or (50), the dispersive term can be written in the familiar MF form as

$$A_{\text{mf}}^{\text{att}}[\{\rho_m(\mathbf{r})\}] = \frac{1}{2} \sum_{i=1}^{n} \sum_{j=1}^{n} \int d\mathbf{r} m_i \rho_i(\mathbf{r}) \int d\mathbf{r}' m_j \rho_j(\mathbf{r}') \times \phi_{ij}^{\text{att}}(|\mathbf{r}-\mathbf{r}'|). \quad (58)$$

The Euler–Lagrange equation for the equilibrium profile of component i in the case of the SAFT-VR MF DFT is now simply given by

$$\mu_i = \mu_{\text{mf},i}^{\text{ref}}(\{\rho_m(\mathbf{r})\}) + \sum_{j=1}^{n} \int d\mathbf{r}' m_i m_j \rho_j(\mathbf{r}') \phi_{ij}^{\text{att}}(|\mathbf{r}-\mathbf{r}'|). \quad (59)$$

These expressions are clearly obtained as a limiting form of Eq. (54) with $g_0^{\text{hs}}[\sigma_x;\overline{\xi_x^{\text{eff}}}(\lambda_{ij};\{\rho_m(\mathbf{r}),\rho_l(\mathbf{r}')\})] \to 1$.

C. The equilibrium density profile and surface tension

The equilibrium density profile is found by solving the Euler–Lagrange relation Eq. (54). Calculations are done considering a planar interface perpendicular to the z axis, where z is the normal distance to the interface. This assumption implies that no density changes are observed in the $x-y$ plane. In fact, we are assuming another MF approximation in our DFT treatment since the density profile is only a function of z on the average, and this is not exact for instantaneous configurations. As a result, the standard DFT approach washes out capillary fluctuations. These fluctuations, which can be viewed as a superposition of sinusoidal surface waves (or two-dimensional normal modes, provided their amplitudes are small), would become increasingly important close to the critical point. These capillary-wave fluctuations are not taken into account explicitly in our treatment, but are not expected to make a significant contribution to the thermodynamic properties of the interface away from the critical region; Henderson[146] has shown that the interfacial tension described by a capillary wave theory is equivalent to the thermodynamic interfacial tension (accessible, e.g., through a DFT treatment) in the case of long wavelength fluctuations.

Two different initial density profiles are proposed as a first trial for each component of the mixture: a hyperbolic tangent and a step function. Normally, a hyperbolic tangent is a more realistic profile and converges faster to the equilibrium profile than a step function. At low temperature, however, the step profile is the best choice since the real density profiles are very steep. The density profiles far from the interfacial region approach asymptotically the bulk density of the homogeneous phases.

The integration space is divided in equal parts with a grid comprising a minimum of 100σ points. The Euler–Lagrange relations are then solved at each point of the interface using a modification of the Powell Hybrid method[147] included in the FORTRAN Minpack routine. Each old density $\rho_i^{(\text{old})}(z_i)$ at a point on the grid denoted by z_i is replaced by a new value $\rho_i^{(\text{new})}(z_i)$ and, when the following point in the interface grid is determined, the new densities for the previous points are used to evaluate the nonlocal term in order to speed up convergence. A whole new profile is generated and the procedure is repeated for a few iterations until there is no significant change between the new and the previous profile. This is done in practice when $|\rho_i^{(\text{new})*}(z_i) - \rho_i^{(\text{old})*}(z_i)| < 10^{-5}$ for all components of the mixture and grid points.

Once the equilibrium density profile is known, the surface tension is determined using the following thermodynamic relation:

$$\gamma = \frac{\Omega + PV}{\mathcal{A}} \quad (60)$$

by integrating the expression for the free-energy density across the interface, where $\mathcal{A}$ is the interfacial area and P is the bulk pressure.

III. RESULTS

The two different versions of our SAFT-DFT have been tested for several specific cases, where the capabilities of the two approaches are examined. Our first goal is to test both approaches and assess the effect of the various assumptions on the calculated density profile and surface tension. In line with the studies of Telo da Gama and co-workers,[64–79] we first examine the fluid-phase behavior and interfacial properties of some model fluid mixtures. Telo da Gama and coworkers predicted the fluid interfacial tension, adsorption and wetting of a number of systems of spherical particles with their simple MF DFT, and studied the effect of varying the relative values of the size and energy parameters on these properties (e.g., see Refs. 69, 70, and 73). Here, we introduce correlations between the particles in the attractive contribution and extend the analysis to mixtures of chain molecules formed from square-well segments (of diameter σ, well-depth $-\epsilon$, and range $\lambda\sigma$) in order to assess the effect of the length asymmetry and other molecular parameters on the interfacial phenomena. The trends observed will be useful in understanding the type of behavior exhibited by real mixtures.

Before describing the interfacial properties of a system, one must first determine the bulk phase equilibrium by solving the equilibrium conditions of equality of temperature,

pressure, and chemical potential for each compound in both phases. Once the equilibrium compositions and densities of the coexisting phases have been determined, it is possible to proceed with a DFT treatment for the corresponding fluid interfaces. In what follows, ϵ is the chosen unit of energy and σ is the unit of length. Accordingly, we define the following reduced quantities in terms of the energy and length parameters of component 1: temperature $T^*=T/(k_B\epsilon_{11})$, pressure $P^*=P\sigma_{11}^3/\epsilon_{11}$, density $\rho^*=\rho\sigma^3$, interfacial thickness $w^*=w/\sigma_{11}$, surface tension $\gamma_{11}^*=\gamma\sigma_{11}^2/\epsilon_{11}$, and distance from the interface $z^*=z/\sigma_{11}$.

A. Square-well fluid mixtures

We consider first a "symmetrical" square-well monomer(1)+dimer(2) nonassociating binary mixture, in which all the segment-segment square-well parameters are the same: $\sigma_{11}=\sigma_{22}=\sigma_{12}$, $\epsilon_{11}=\epsilon_{22}=\epsilon_{12}$, and $\lambda_{11}=\lambda_{22}=\lambda_{12}=1.50$. The adequacy of the SAFT-VR theory in describing the bulk fluid-phase behavior for this system has already been assessed by comparison with Gibbs ensemble Monte Carlo simulation.[148] Since the conformal and nonconformal molecular parameters of the segments forming both molecules are the same, such systems of monomers and chains are representative models to identify the effect of molecular shape (chain length) of one of the components on the interfacial properties. In particular, by changing the number of segments in the chain, these systems are prototype models for studies of the interfacial properties of mixtures comprising members of homologous series such as the *n*-alkanes or *n*-perfluoroalkanes with increasing differences in the molecular weights between the two species.

The vapor-liquid equilibrium at a selected reduced temperature of $T^*=k_BT/\epsilon=1.2$ is shown in Fig. 1(a). Once the fluid-phase equilibrium has been determined (using a standard numerical procedure), the behavior at the interface can be studied by applying our SAFT-DFT procedure. The dependence of the surface tension on the monomer composition as calculated from both approaches is depicted in Fig. 1(b). The MF approximation leads to lower surface tension values than an approach in which correlations are included in the attractive perturbation term. The missing contribution from the correlation function is responsible for this effect. It can also be seen that the difference between the vapor-liquid tension increases as the composition approaches the pure dimer value. This result is in agreement with the calculations performed for pure square-well fluids and real compounds in previous work,[59,60] where lower values of the surface tension with the MF approach were also obtained.

More information about the interface may be obtained by checking the density and composition profiles of this mixture. A point at fixed pressure is chosen from the pressure-composition (Px) slice [dashed line in Fig. 1(a)] and the profiles for each component in the vicinity of the vapor-liquid interface are calculated. The separate density and composition profiles of the monomer and the dimer predicted with the MF and full DFT versions of the theory are presented in Figs. 2(a) and 2(b), respectively. Some interesting conclusions can be gleaned from these results. First of all,

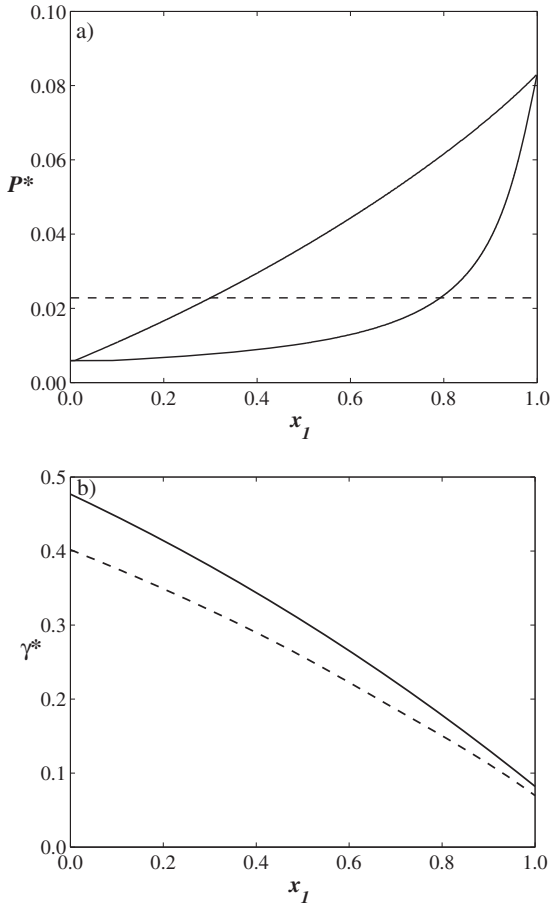

FIG. 1. (a) Pressure-composition (Px) slice and (b) interfacial tension $\gamma^*=\gamma\sigma_{11}^2/\epsilon_{11}$ as a function of the composition x_1 for the vapor-liquid equilibria of a square-well monomer(1)+dimer(2) binary mixture, with $\sigma_{11}=\sigma_{22}$, $\epsilon_{11}=\epsilon_{22}$, and $\lambda_{11}=\lambda_{22}=1.50$ at a reduced temperature of $T^*=1.2$. The continuous curves correspond to the predictions from the full SAFT-VR DFT approach and the dashed curves in (b) to the SAFT-VR DFT treatment.

the differences between the profiles obtained from both approaches are not marked, with the profile corresponding to the MF approach being slightly sharper. Second, it is clear that the profiles are monotonic with no evidence of adsorption or desorption in the case of the monomer-dimer mixture. This could have been expected considering the moderate length asymmetry between the two components of the mixture. It is important to point out that very tiny differences in the density and composition profiles lead to notable variations in the surface tension. As a consequence, a very accurate determination of the profiles is crucial for an accurate calculation of the interfacial properties.

The influence of the chain length on the density profiles and surface tension of mixtures of chainlike molecules is summarized in Fig. 3. We keep fixed the chain length of the first component fixed as a monomer ($m_1=1$) and vary the number of segments of the second component by increasing the number of segments in the chain ($m_2=2$, 3, and 4). Following the same procedure as for the monomer-dimer system, the phase equilibrium is calculated at the same reduced temperature for each of the systems. The corresponding Px slices are shown in Fig. 3(a). As expected, when the chain length of the second compound is increased, the proportion of the chain in the gas phase decreases markedly, resulting in wider phase envelopes.

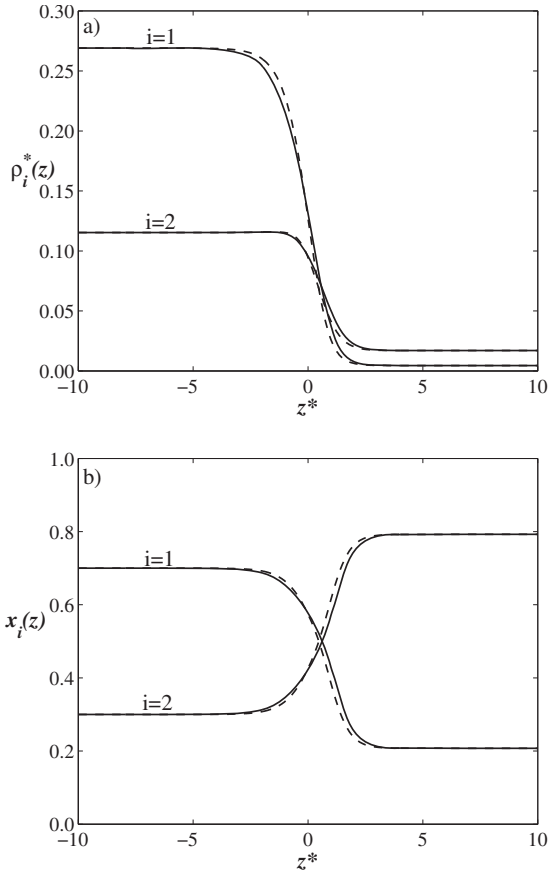

FIG. 2. (a) Density profiles $\rho_1^*(z)=\rho_1(z)\sigma_{11}^3$ and $\rho_2^*(z)=\rho_2(z)\sigma_{11}^3$ as functions of the distance from the interface $z^*=z/\sigma_{11}$ and (b) composition profiles $x_1(z)$ and $x_2(z)$ as functions of z^* for the vapor-liquid interface of a square-well monomer(1)+dimer(2) binary mixture with $\sigma_{11}=\sigma_{22}$, $\epsilon_{11}=\epsilon_{22}$, and $\lambda_{11}=\lambda_{22}=1.50$ at a reduced temperature of $T^*=1.2$. The composition of the coexisting liquid phase is $x_1=0.3$ in (a) and (b). Curves labeled as in Fig. 1.

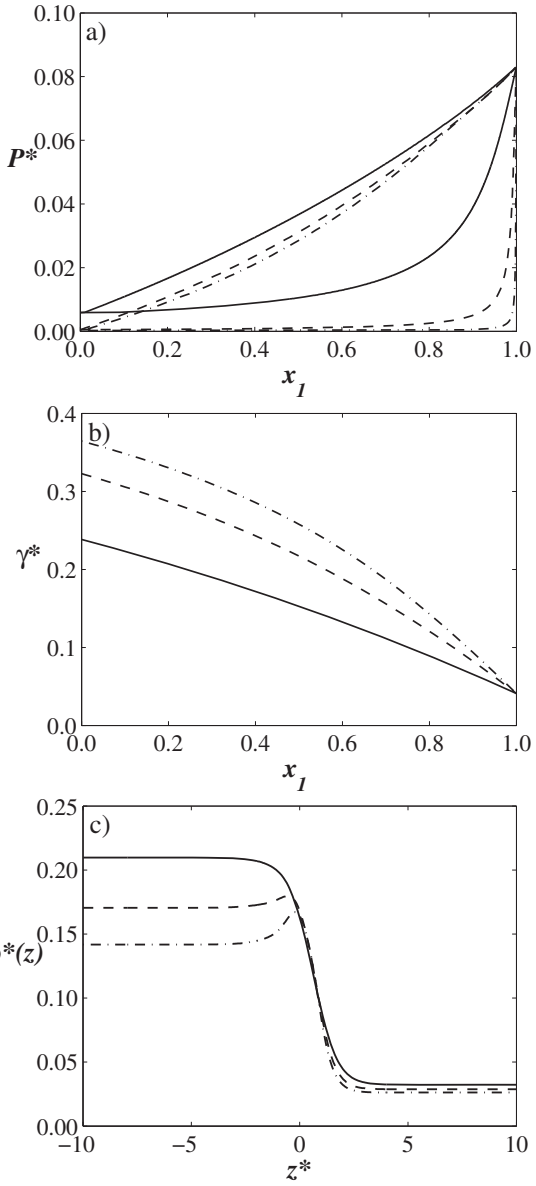

FIG. 3. (a) Pressure-composition (Px) slice, (b) interfacial tension as a function of the composition x_1, and (c) density profile $\rho^*(z)=\rho(z)\sigma_{11}^3$ as a function of the distance from the interface $z^*=z/\sigma_{11}$ for the vapor-liquid equilibria of square-well monomer(1)+dimer(2) (continuous curves), monomer(1)+trimer(2) (dashed curves), and monomer(1)+tetramer(2) (dotted-dashed curves) binary mixtures, with $\sigma_{11}=\sigma_{22}$, $\epsilon_{11}=\epsilon_{22}$, and $\lambda_{11}=\lambda_{22}=1.50$ at a reduced temperature of $T^*=1.2$, obtained from the SAFT-VR DFT approach. The composition of the coexisting liquid phase is $x_1=0.5$ in (c).

The dependence of the surface tension of the three mixtures on composition is shown in Fig. 3(b). The surface tension converges to that of the pure monomer in all cases as $x_1 \to 1$. When the composition of the second compound is increased, the surface tension becomes larger as the mixture becomes more asymmetric, an expected result as the difference between the densities and compositions of the liquid and vapor phases becomes more significant as the chain-length asymmetry is increased. It is also worth noting that the composition dependence of the surface tension of the monomer(1)+dimer(2) binary mixture is almost linear, with the curvature increasing when the chain length of the second compound is increased.

The density profiles of these three binary mixtures have also been examined in detail for an equimolar composition ($x_1=0.5$). As can be seen in Fig. 3(c), the density profile of the monomer(1)+dimer(2) mixture is characterized by a monotonic behavior (as previously shown in Fig. 2). A small adsorption of the monomer at the interface is observed in the case of the most asymmetric mixture studied [monomer(1)+tetramer(2)]. The monomer molecules tend to accumulate at the interface on increasing the chain length of the second compound. We have also assessed the influence of the composition where it appears that the maximum degree of adsorption occurs for the equimolar liquid mixture. This type of enhanced adsorption of one component relative to the other is seen in binary mixtures of spherical molecules when there are significant differences in the values of the unlike dispersion interactions (e.g., see Refs. 62, 66, 67, and 73).

The other parameter that defines the volume of a molecule is the segment size or diameter. For completeness, we have determined the interfacial properties of mixtures of spherical square-well molecules of different diameter. In particular, we consider two monomer mixtures, with segment size ratios σ_{22}/σ_{11} of 1.5 and 2.0. The (a) vapor-liquid Px slice and (b) the interfacial tension as a function of composition at $T^*=1.2$ is depicted in Fig. 4. It is clear from Fig. 4(a) that the influence of an asymmetry in the ratio σ_{22}/σ_{11}

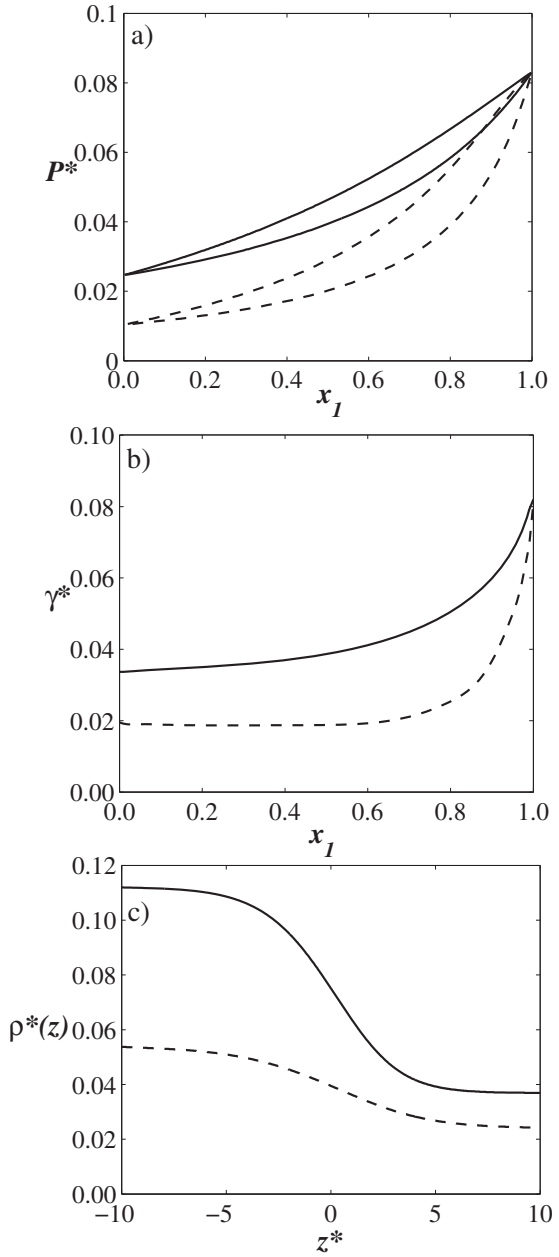

FIG. 4. (a) Pressure-composition (Px) slice, (b) interfacial tension $\gamma^* = \gamma\sigma_{11}^2/\epsilon_{11}$ as a function of the composition x_1, and (c) density profile $\rho^*(z)=\rho(z)\sigma_{11}^3$ as a function of the distance from the interface $z^*=z/\sigma_{11}$ for the vapor-liquid equilibria of square-well monomer(1)+monomer(2) binary mixtures with $\epsilon_{11}=\epsilon_{22}$, $\lambda_{11}=\lambda_{22}=1.50$, $\sigma_{22}/\sigma_{11}=1.5$ (continuous curves), and $\sigma_{22}/\sigma_{11}=2.0$ (dashed curves) at a reduced temperature of $T^*=1.2$, obtained from the SAFT-VR DFT approach. The composition of the coexisting liquid phase is $x_1=0.5$ in (c).

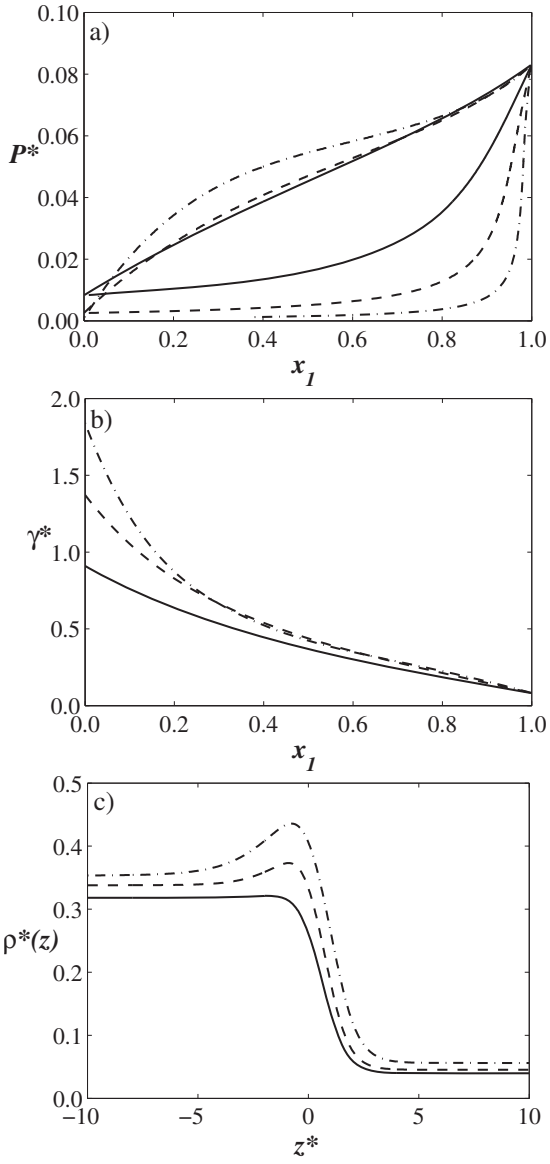

FIG. 5. (a) Pressure-composition (Px) slice, (b) interfacial tension $\gamma^* = \gamma\sigma_{11}^2/\epsilon_{11}$ as a function of the composition x_1, and (c) density profile $\rho^*(z)=\rho(z)\sigma_{11}^3$ as a function of the distance from the interface $z^*=z/\sigma_{11}$ for the vapor-liquid equilibria of square-well monomer(1)+monomer(2) binary mixtures with $\sigma_{11}=\sigma_{22}$, $\lambda_{11}=\lambda_{22}=1.50$, $\epsilon_{11}/\epsilon_{22}=1.5$ (continuous curves), and $\epsilon_{11}/\epsilon_{22}=2.0$ (dashed curves) at a reduced temperature of $T^*=1.2$, obtained from the SAFT-VR DFT approach. The composition of the coexisting liquid phase is $x_1=0.2$ in (c).

on the phase behavior is less marked than that corresponding to the chain length. In addition, the phase envelope of both mixtures is narrower over the whole range of compositions when compared with that shown in Fig. 2(a). As a consequence, one would expect a lower surface tension as can be seen in Fig. 4(b). The surface tension of the mixture decreases when the segment size ratio is increased. The effect is most marked at high concentrations of the smaller molecule. In Fig. 4(c), the density profiles corresponding to the smallest molecule for both mixtures are compared and no adsorption phenomenon is observed in this case, confirming that the influence of this parameter is less significant. The broad density profile obtained for the mixture with $\sigma_{22}/\sigma_{11}=2.0$ indicates the system is in the vicinity of the critical point, as the difference between the gas and the liquid densities is very small.

We have also analyzed the influence of the attractive dispersion energy on the interfacial properties. In Fig. 5, we undertake a similar analysis for three different binary mixtures of spherical molecules of the same size with different dispersive energy ratios, $\epsilon_{22}/\epsilon_{11}=1.50$, 1.75, and 2.00 at $T^*=1.2$. The phase envelope of the mixture as a function of the dispersive energy ratio is shown in Fig. 5(a). As the dispersive energy ratio is increased the phase envelopes become wider, as one would expect. In Fig. 5(b), the calculated sur-

face tension is seen to exhibit similar values over a wide range of compositions, for mole fractions of component 1 from about 0.4 to 1.0. As the composition approaches that of the pure component 2, the surface tension increases very sharply: the surface tension value of the mixture with $\epsilon_{22}/\epsilon_{11}=2.0$ is twice that of the mixture with $\epsilon_{22}/\epsilon_{11}=1.50$ as $x_1 \to 0$. It is evident that the difference in dispersive energy plays a key role in the interfacial behavior and is most significant as the composition approaches that of the component with the highest dispersive energy. The corresponding density profiles corroborate that a marked adsorption phenomena is associated with this range of composition. In Fig. 5(c), we show the density profiles of the mixtures with different dispersion interactions at a selected initial liquid composition of $x_1=0.20$. As can be seen, the adsorption phenomenon is most significant when the dispersive energy ratio $\epsilon_{22}/\epsilon_{11}$ is increased. This is consistent with the results obtained by Telo da Gama and co-workers[64–79] with a MF DFT.

To end our analysis of the effect of the intermolecular parameters on the interfacial properties, we study the effect of changing the range of the attractive square well in binary mixtures of spherical particles. In particular, we consider binary mixtures for two different ratios of the potential range, $\lambda_{22}/\lambda_{11}=1.50/1.25$ and 1.75/1.25, at a reduced temperature of $T^*=1.2$. The Px slice determined at this temperature is depicted in Fig. 6(a), from which one can see that for the selected thermodynamic conditions, the system is above the critical temperature of component 1, with a very small fluid-phase envelope for one of the mixtures. This clearly has an important effect on the surface tension of the mixture, as shown in Fig. 6(b). The vapor-liquid surface tension predicted for the mixture with $\lambda_{22}/\lambda_{11}=1.50/1.25$ is relatively small, while larger values are found for the mixture with a range ratio of 1.75/1.25. It is instructive to examine the density profiles of the compound with the larger potential range. We have chosen to calculate the profile at an initial liquid composition of $x_1=0.10$ to ensure that we are inside the fluid-phase envelope in both cases. The mixture with the potential range ratio of $\lambda_2/\lambda_1=1.50/1.25$ is very close to the critical point at the chosen state point, and hence one obtains a very smooth profile with no marked adsorption. However, the mixture with the potential range ratio of 1.75/1.25 exhibits a strong degree of asymmetry with a correspondingly marked adsorption in the density profile.

It is clear that surface tension, as the other thermodynamic and structural properties, is affected by all of the molecular parameters. From our current analysis, it would appear that the chain length, the dispersive energy, and the range of the intermolecular potential have a more significant effect on the interfacial properties, while the size of the segments making up the molecules does not contribute to the same degree.

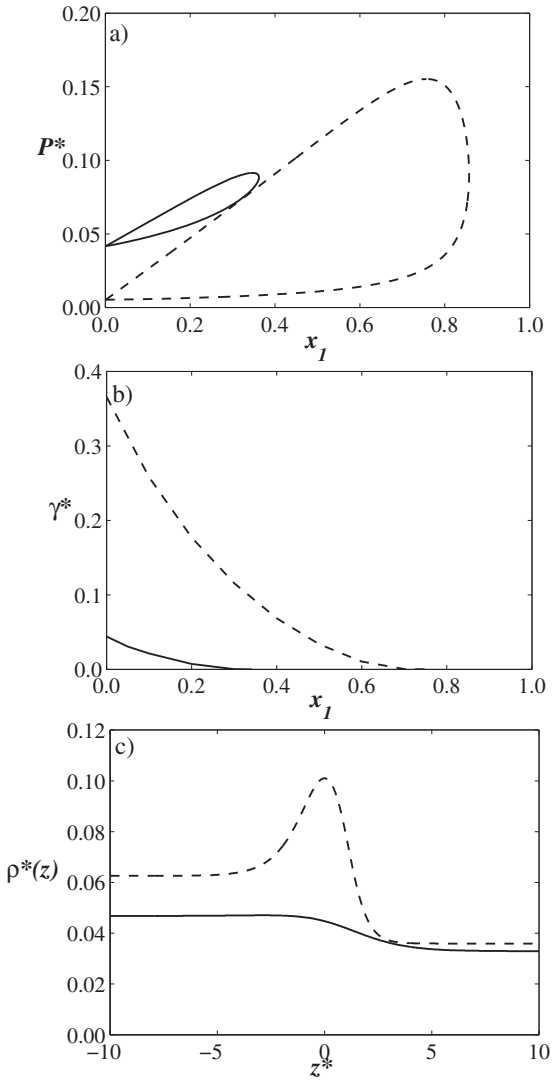

FIG. 6. (a) Pressure-composition (Px) slice, (b) interfacial tension $\gamma^*=\gamma\sigma_{11}^2/\epsilon_{11}$ as a function of the composition x_1, and (c) density profile $\rho^*(z)=\rho(z)\sigma_{11}^3$ as a function of the distance from the interface $z^*=z/\sigma_{11}$ for the vapor-liquid equilibria of square-well monomer(1)+monomer(2) binary mixtures, with $\sigma_{11}=\sigma_{22}$, $\epsilon_{11}=\epsilon_{22}$, $\lambda_{11}=1.25$, $\lambda_{22}=1.50$ (continuous curves), and $\lambda_{22}=1.75$ (dashed curves) at a reduced temperature of $T^*=1.2$, obtained from the SAFT-VR DFT approach. The composition of the coexisting liquid phase is $x_1=0.1$ in (c).

B. Binary mixtures of *n*-alkanes

The valuable information extracted from the previous analysis with model systems provides a basis from which to understand the interfacial behavior of real mixtures. In this section, we apply the same formalism to predict some interfacial properties of real *n*-alkane mixtures. In order to assess the capability of the theory in predicting these properties, we compare the theoretical predictions with the available experimental data. We study the interfacial properties of two different binary *n*-alkane mixtures to understand, from a molecular perspective, the effect on the interfacial profiles of increasing the asymmetry in the chain length between the components of the mixture.

We first consider the methane(1)+propane(2) binary mixture. Linear *n*-alkanes are modeled as homonuclear chainlike molecules comprising m_i square-well segments of diameter σ_{ii}, dispersive energy ϵ_{ii}, and intermolecular potential range λ_{ii}. The molecular parameters of the pure components have been previously obtained with the SAFT-VR equation of state by fitting the saturated liquid densities and vapor pressures along the vapor-liquid coexistence range. We use the reported values of the parameters[118] to calculate the

TABLE I. Square-well segment-segment intermolecular molecular parameters of the compounds examined in our study with the SAFT-VR approach (Ref. 118).

Compound	M_w (g/mol)	m	σ (Å)	ϵ/k_B (K)	λ
CH_4	16.04	1.000	3.6847	167.30	1.4479
C_3H_8	44.10	1.667	3.8899	260.91	1.4537
$C_{10}H_{22}$	142.28	4.000	3.9675	247.08	1.5925

interfacial profiles and the fluid interfacial tension of the mixtures. The values of the molecular parameter used in this work are summarized in Table I for completeness. As the components of the mixture are very similar, we use the traditional Lorentz and Berthelot combining rules for the unlike segment size, dispersive energy, and potential range [cf. Eqs. (2)–(4), where $k_{ij}=0$]. This mixture exhibits type I phase behavior according to the Scott and van Konynenburg classification of binary mixtures,[149,150] and therefore only vapor-liquid phase separation is expected for the entire fluid range of temperatures and pressures. In Fig. 7(a), we show the Px slices for the methane(1)+propane(2) binary mixture at different temperatures. As can be seen, the agreement between the SAFT-VR predictions for the vapor-liquid equilibria and the experimental data is good over the whole range of pressures apart from the expected inadequacy in the vicinity of the critical point. The dependence of the calculated vapor-liquid interfacial tension on the composition for the corresponding temperatures is shown in Fig. 7(b). Here we consider two different theoretical levels of approximation: the full SAFT-VR DFT and the SAFT-VR MF DFT treatments (see Secs. II B 1 and II B 2). In both cases, accurate predictions are obtained considering that no further adjustment of the parameters obtained from a description of the bulk fluid phase behavior is made. The theoretical predictions for the interfacial tension are in good agreement with experimental data in all cases, excepting in the critical region where one overestimates the critical temperature, due to the lack of a renormalization-group treatment.[151] The SAFT-VR DFT treatment which incorporates the correlations in the attractive perturbation is seen to perform slightly better at low temperatures, as one would have expected based on the results obtained for pure fluids.[60]

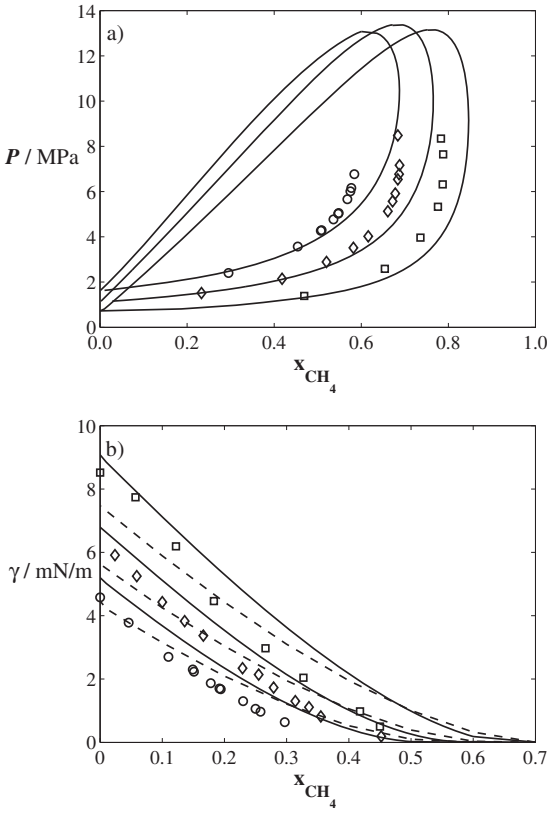

FIG. 7. (a) Pressure-composition (Px) slices at temperatures of $T=283$ K (squares), $T=303$ K (diamonds), and 318 K (circles), and (b) interfacial tension as a function of the composition x_1 for the vapor-liquid equilibria of the methane(1)+propane(2) binary mixture compared with the SAFT-VR DFT predictions. The symbols represent the existing experimental data (Ref. 17) and the curves represent the theoretical predictions from the full SAFT-VR DFT (continuous curves) and the SAFT-VR MF DFT (dashed curves).

We now examine a more asymmetric binary mixture of n-alkanes to assess the adequacy of the theory in predicting the interfacial properties of these more extreme cases. The methane(1)+n-decane(2) binary mixture is considered as a good prototype of asymmetric mixtures of n-alkanes. In particular, we use the previously reported molecular parameters of n-decane.[118] As can be seen from Fig. 8(a), the SAFT-VR approach is still able to provide a reasonably good description of the asymmetric phase envelope of the mixture without using a binary parameter ($k_{ij}=0$). We have also obtained the surface tension of the mixture, as a function of pressure, along the vapor-liquid coexistence envelope, as shown in Fig. 8(b). The SAFT-VR DFT provides a very accurate prediction of the experimental surface tension[152] over the whole range of pressures, except near the critical region.

The density profiles calculated for the two systems considered, i.e., the methane(1)+propane(2) and methane(1)+n-decane(2) binary mixtures, at the same thermodynamic conditions are also compared in Fig. 9. This provides a molecular perspective of the difference in the adsorption behavior of mixtures with different chain-length asymmetry. While there is little adsorption of methane in the interface of the first methane(1)+propane(2) mixture, the density profile corresponding to the methane(1)+n-decane(2) mixture exhibits a marked adsorption of methane at the fluid interface. The results characterizing Figs. 9(a) and 9(b) were already expected from our studies of the model systems (Sec. III A) considering the increasing of asymmetry of the mixture when passing from propane to n-decane. In the methane(1)+n-decane(2) system, it is clearly thermodynamically favorable for the methane molecules to accumulate at the interface, a direct consequence of the decreasing miscibility of

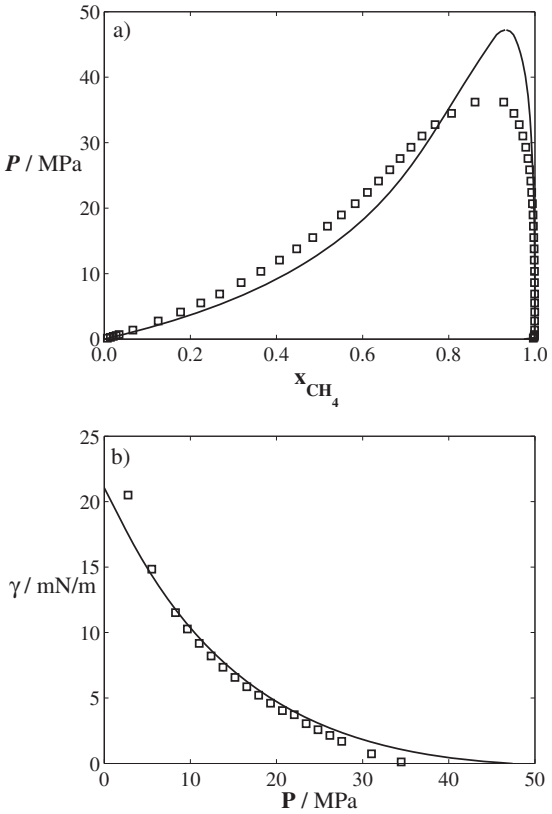

FIG. 8. (a) Pressure-composition (Px) slice and (b) interfacial tension as a function of the pressure for the vapor-liquid equilibria of the methane(1)+n-decane(2) binary mixture at a temperature of $T=311$ K compared with the SAFT-VR DFT predictions. The symbols represent the existing experimental data (Ref. 152) and the curve the theoretical predictions from the full SAFT-VR DFT.

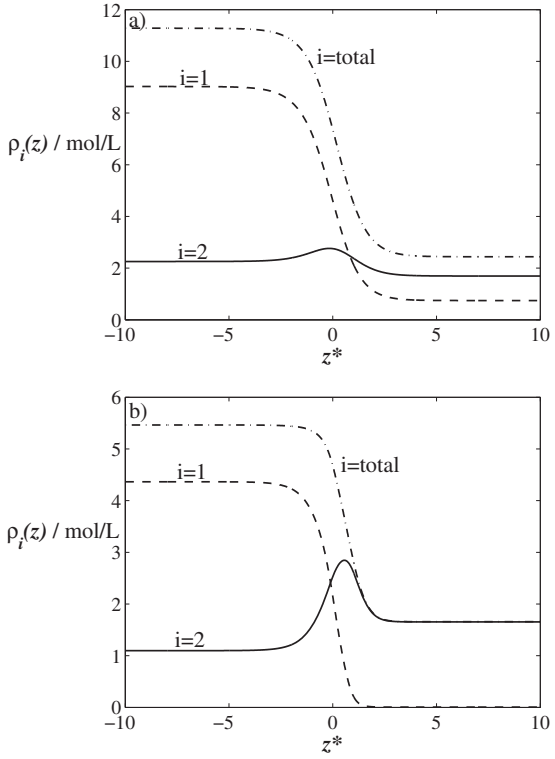

FIG. 9. Density profiles $\rho_1(z)$, $\rho_2(z)$, and $\rho(z)$ as functions of the distance from the interface $z^*=z/\sigma_{11}$ at a temperature of $T=311$ K and a liquid composition of $x_1=0.20$, obtained from the SAFT-VR DFT approach for the vapor-liquid equilibria of the (a) methane(1)+propane(2), and (b) methane(1)+n-decane(2) binary mixtures.

methane in n-alkanes of increasing molecular weight. Finally, in Figs. 10(a) and 10(b), we show the composition profiles of both mixtures. Both profiles exhibit a monotonic behavior. As can be seen, the profiles corresponding to the methane+n-decane binary mixture are very sharp since the equilibrium conditions are far removed from the critical point, corresponding to a vapor phase which is nearly pure methane. It is important to note that though most of the results presented here correspond to the predictions from the full SAFT-VR DFT approach, the SAFT-VR MF DFT treatment also adequately describes the surface tension and adsorption phenomena of these real mixtures.

IV. CONCLUSIONS

We have extended the general SAFT-VR DFT formalism originally developed for pure fluids[59,60] to deal with the interfacial properties of multicomponent systems of associating chain molecules. In order to construct a tractable DFT, a number of approximations, at different levels, are made to estimate the various contributions to the Helmholtz free-energy functional. Two different approaches have been followed to incorporate the segment-segment correlations by retaining the radial distribution function in the attractive term: a MF version (SAFT-VR MF DFT) and a more rigorous approach where the distribution function is evaluated at an average density along the profile (SAFT-VR DFT).

The new approach has been used to study the influence of the molecular parameters on the interfacial phenomena for some representative model systems. Enhanced adsorption in the interface is found on increasing the asymmetry of the components in the mixture. In particular, the density profiles and interfacial tension are seen to be very sensitive to the relative chain lengths, the dispersive energies, and the ranges of the attractive potential. Such an analysis provides a molecular based understanding of the microscopic features that control the interfacial behavior of mixtures of chainlike molecules.

The SAFT-VR DFT approach has been used to predict the vapor-liquid interfacial properties of real n-alkane binary mixtures. In particular, we have determined the interfacial properties of methane+propane and the more asymmetrical methane+n-decane binary mixtures. Agreement between the theoretical predictions and existing experimental data for the vapor-liquid interfacial tension is very good, particularly if one considers that the molecular parameters are obtained solely from a description for the bulk fluid-phase behavior without further refinement. The full SAFT-VR DFT provides a superior performance than the SAFT-VR MF DFT version, especially at low temperatures, though the description with the latter is still reasonable for the systems examined in this work.

The theoretical framework developed in this work opens up a wide variety of possibilities, enabling a determination of the interfacial properties of complex fluids in a reliable and fully predictive manner. We are now embarking on challeng-

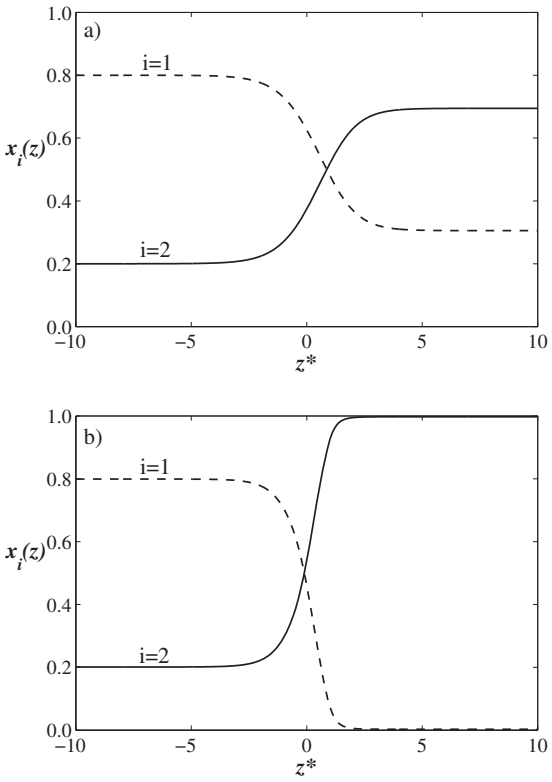

FIG. 10. Composition profiles $x_1(z)$ and $x_2(z)$ as functions of the distance from the interface $z^*=z/\sigma_{11}$ at a temperature of $T=311$ K and a liquid composition of $x_1=0.20$, obtained from the SAFT-VR DFT approach for the vapor-liquid equilibria of the (a) methane(1)+propane(2) and (b) methane(1)+*n*-decane(2) binary mixtures.

ing extensions of the theory to describe the interfacial properties of mixtures of chain molecules including colloid-polymer systems[153,154] and liquid crystals,[155–157] which can be described within this type of formalism.

ACKNOWLEDGMENTS

F.J.B. acknowledges the financial support from the Spanish Dirección General de Investigación (Project No. FIS2007-66079-C02-02) and the Proyecto de Excelencia from Junta de Andalucía (Grant No. P07-FQM02884). Support from Universidad de Huelva and Junta de Andalucía is also acknowledged. F.L. thanks Shell for funding a research fellowship. Additional funding from the Engineering and Physical Sciences Research Council of the U.K. (EPSRC Grant No. EP/E016340) is also gratefully acknowledged by the Molecular Systems Engineering Group, as is the award of a refurbishment grant for the Royal Society-Wolfson Foundation.

[1] W. G. Chapman, K. E. Gubbins, G. Jackson, and M. Radosz, Fluid Phase Equilib. **52**, 31 (1989).
[2] W. G. Chapman, K. E. Gubbins, G. Jackson, and M. Radosz, Ind. Eng. Chem. Res. **29**, 1709 (1990).
[3] M. S. Wertheim, J. Stat. Phys. **35**, 35 (1984).
[4] M. S. Wertheim, J. Stat. Phys. **42**, 459 (1986).
[5] M. S. Wertheim, J. Stat. Phys. **42**, 477 (1986).
[6] A. Gil-Villegas, A. Galindo, P. J. Whitehead, S. J. Mills, G. Jackson, and A. N. Burgess, J. Chem. Phys. **106**, 4168 (1997).
[7] A. Galindo, L. A. Davies, A. Gil-Villegas, and G. Jackson, Mol. Phys. **93**, 241 (1998).
[8] F. J. Blas and L. F. Vega, Mol. Phys. **92**, 135 (1997).
[9] J. Gross and G. Sadowski, Ind. Eng. Chem. Res. **40**, 1244 (2001).
[10] A. Lymperiadis, C. S. Adjiman, A. Galindo, and G. Jackson, J. Chem. Phys. **127**, 234903 (2007).
[11] A. Lymperiadis, C. S. Adjiman, G. Jackson, and A. Galindo, Fluid Phase Equilib. **274**, 85 (2008).
[12] E. A. Müller and K. E. Gubbins, Ind. Eng. Chem. Res. **40**, 2193 (2001).
[13] I. G. Economou, Ind. Eng. Chem. Res. **41**, 953 (2002).
[14] P. Paricaud, A. Galindo, and G. Jackson, Fluid Phase Equilib. **194–197**, 87 (2002).
[15] S. Tan, H. Adidharma, and M. Radosz, Ind. Eng. Chem. Res. **47**, 8063 (2002).
[16] D. B. Macleod, Trans. Faraday Soc. **19**, 38 (1923).
[17] C. F. Weinaug and D. L. Katz, Ind. Eng. Chem. **35**, 239 (1943).
[18] R. H. Fowler, Proc. R. Soc. London, Ser. A **159**, 229 (1937).
[19] E. A. Guggenheim, J. Chem. Phys. **13**, 253 (1945).
[20] Y. X. Zuo and E. H. Stendby, Can. J. Chem. Eng. **75**, 1130 (1997).
[21] J. D. van der Waals, Z. Phys. Chem. **13**, 657 (1894).
[22] J. W. Strutt (Lord Rayleigh), Philos. Mag. **33**, 209 (1892).
[23] J. W. Cahn and J. E. Hilliard, J. Chem. Phys. **28**, 258 (1958).
[24] J. S. Rowlinson and B. Widom, *Molecular Theory of Capillarity* (Clarendon, Oxford, 1982).
[25] B. S. Carey, Ph.D. thesis, University of Minnesota, 1979.
[26] B. S. Carey, H. T. Davis, and L. E. Scriven, AIChE J. **26**, 705 (1980).
[27] C. I. Poser and I. C. Sanchez, Macromolecules **14**, 361 (1981).
[28] P. M. W. Cornelisse, C. J. Peters, and J. de Swaan Arons, Fluid Phase Equilib. **82**, 119 (1993).
[29] P. M. W. Cornelisse, C. J. Peters, and J. de Swaan Arons, Fluid Phase Equilib. **117**, 312 (1996).
[30] P. M. W. Cornelisse, C. J. Peters, and J. de Swaan Arons, Mol. Phys. **80**, 941 (1993).
[31] P. M. W. Cornelisse, C. J. Peters, and J. de Swaan Arons, Int. J. Thermophys. **19**, 1501 (1998).
[32] P. M. W. Cornelisse, M. Wijtkamp, C. J. Peters, and J. de Swaan Arons, Fluid Phase Equilib. **150–151**, 633 (1998).
[33] L. E. Urlic, L. J. Florusse, E. J. M. Straver, S. Degrange, and C. J. Peters, Transp. Porous Media **52**, 141 (2003).
[34] C. Miqueu, B. Mendiboure, A. Gracia, and J. Lachaise, Fluid Phase Equilib. **218**, 189 (2004).
[35] C. Miqueu, B. Mendiboure, A. Gracia, and J. Lachaise, Ind. Eng. Chem. Res. **44**, 3321 (2005).
[36] C. Miqueu, B. Mendiboure, A. Gracia, and J. Lachaise, Fuel **87**, 612 (2008).
[37] H. Lin, Y. Duan, and Q. Min, Fluid Phase Equilib. **254**, 75 (2007).
[38] A. Mejía, H. Segura, L. F. Vega, and J. Wisniak, Fluid Phase Equilib. **227**, 225 (2005).
[39] A. Mejia, H. Segura, J. Wisniak, and I. Polishuk, J. Phase Equilib. Diffus. **26**, 1 (2005).
[40] A. Mejía and H. Segura, Int. J. Thermophys. **25**, 1395 (2004).
[41] A. Mejía and H. Segura, Int. J. Thermophys. **26**, 13 (2005).
[42] A. Mejía, J. C. Pamies, D. Duque, H. Segura, and L. F. Vega, J. Chem. Phys. **123**, 034505 (2005).
[43] A. Mejía and L. F. Vega, J. Chem. Phys. **124**, 244505 (2006).
[44] H. Kahl and S. Enders, Fluid Phase Equilib. **172**, 27 (2000).
[45] H. Kahl and S. Enders, Phys. Chem. Chem. Phys. **4**, 931 (2002).
[46] S. Enders, H. Kahl, and J. Winkelmann, Fluid Phase Equilib. **228–229**, 511 (2005).
[47] S. Enders and H. Kahl, Fluid Phase Equilib. **263**, 160 (2008).
[48] O. G. Nino-Amezquita, S. Enders, P. T. Jaeger, and R. Eggers, Ind. Eng. Chem. Res. **49**, 592 (2010).
[49] M. B. Oliveira, I. M. Marrucho, J. A. P. Coutinho, and A. J. Queimada, Fluid Phase Equilib. **267**, 83 (2008).
[50] D. Fu and Y. Wei, Ind. Eng. Chem. Res. **47**, 4490 (2008).
[51] X. S. Li, J. M. Liu, and D. Fu, Ind. Eng. Chem. Res. **47**, 8911 (2008).
[52] D. Fu, H. J. Jian, and B. S. Wang, Fluid Phase Equilib. **279**, 136 (2009).
[53] E. A. Müller and A. Mejia, Fluid Phase Equilib. **282**, 68 (2009).
[54] G. Galliero, M. M. Piñeiro, B. Mendiboure, C. Miqueu, T. Lafitte, and D. Bessieres, J. Chem. Phys. **130**, 104704 (2009).
[55] R. Evans, "Density functionals in the theory of nonuniform fluids," in *Fundamentals of Inhomogeneous Fluids* (Dekker, New York, 1992).
[56] H. T. Davis, *Statistical Mechanics of Phases, Interfaces and Thin Films* (VCH, Weinheim, 1996).
[57] F. J. Blas, E. M. del Rio, E. de Miguel, and G. Jackson, Mol. Phys. **99**, 1851 (2001).

[58] G. J. Gloor, F. J. Blas, E. M. del Rio, E. de Miguel, and G. Jackson, Fluid Phase Equilib. **194–197**, 521 (2002).
[59] G. J. Gloor, G. Jackson, F. J. Blas, E. M. del Rio, and E. de Miguel, J. Chem. Phys. **121**, 12740 (2004).
[60] G. J. Gloor, G. Jackson, F. J. Blas, E. M. del Rio, and E. de Miguel, J. Phys. Chem. C **111**, 15513 (2007).
[61] J. Gross, J. Chem. Phys. **131**, 204705 (2009).
[62] D. E. Sullivan, J. Chem. Phys. **25**, 1669 (1982).
[63] D. E. Sullivan, J. Chem. Phys. **77**, 2632 (1982).
[64] M. M. Telo da Gama and R. Evans, Mol. Phys. **41**, 1091 (1980).
[65] M. M. Telo da Gama and R. Evans, Faraday Symp. Chem. Soc. **16**, 45 (1981).
[66] M. M. Telo da Gama and R. Evans, Mol. Phys. **48**, 229 (1983).
[67] M. M. Telo da Gama and R. Evans, Mol. Phys. **48**, 251 (1983).
[68] M. M. Telo da Gama and R. Evans, Mol. Phys. **48**, 687 (1983).
[69] P. Tarazona, M. M. Telo da Gama, and R. Evans, Mol. Phys. **49**, 283 (1983).
[70] P. Tarazona, M. M. Telo da Gama, and R. Evans, Mol. Phys. **49**, 301 (1983).
[71] M. M. Telo da Gama, R. Evans, and I. Hadjiagapiou, Mol. Phys. **52**, 573 (1984).
[72] D. J. Lee, M. M. Telo da Gama, and K. E. Gubbins, Mol. Phys. **53**, 1113 (1984).
[73] D. J. Lee, M. M. Telo da Gama, and K. E. Gubbins, J. Phys. Chem. **89**, 1514 (1985).
[74] M. M. Telo da Gama and K. E. Gubbins, Mol. Phys. **59**, 227 (1986).
[75] M. M. Telo da Gama and J. H. Thurtell, J. Chem. Soc., Faraday Trans. 2 **82**, 1721 (1986).
[76] M. M. Telo da Gama, Mol. Phys. **62**, 585 (1987).
[77] J. Aracil, G. Luengo, B. S. Almeida, M. M. Telo da Gama, R. G. Rubio, and M. D. Pena, J. Phys. Chem. **93**, 3210 (1989).
[78] B. S. Almeida and M. M. Telo da Gama, J. Phys. Chem. **93**, 4132 (1989).
[79] P. I. C. Teixeira, B. S. Almeida, M. M. Telo da Gama, J. A. Rueda, and R. G. Rubio, J. Phys. Chem. **96**, 8488 (1992).
[80] R. Penfold, J. Satherley, and S. Nordholm, Fluid Phase Equilib. **109**, 183 (1995).
[81] S. Sarman, H. Greberg, J. Satherley, R. Penfold, and S. Nordholm, Fluid Phase Equilib. **172**, 145 (2000).
[82] H. Greberg, G. V. Paolini, J. Satherley, R. Penfold, and S. Nordholm, J. Colloid Interface Sci. **235**, 334 (2001).
[83] P. Bryk, K. Bucior, and S. Sokolowski, J. Phys. Chem. C **111**, 15523 (2007).
[84] Y. X. Yu and J. Z. Wu, J. Chem. Phys. **117**, 2368 (2002).
[85] Y. Rosenfeld, Phys. Rev. Lett. **63**, 980 (1989).
[86] R. Roth, R. Evans, A. Lang, and G. Kahl, J. Phys.: Condens. Matter **14**, 12063 (2002).
[87] Y. X. Yu and J. Z. Wu, J. Chem. Phys. **117**, 10156 (2002).
[88] S. Tripathi and W. G. Chapman, J. Chem. Phys. **122**, 094506 (2005).
[89] A. Dominik, S. Tripathi, and W. G. Chapman, Ind. Eng. Chem. Res. **45**, 6785 (2006).
[90] S. Jain, A. Dominik, and W. G. Chapman, J. Chem. Phys. **127**, 244904 (2007).
[91] S. Jain and W. G. Chapman, Mol. Phys. **107**, 1 (2009).
[92] J. Winkelmann, J. Phys.: Cond. Matt. **13**, 4739 (2001).
[93] H. Kahl, M. Mecke, and J. Winkelmann, Fluid Phase Equilib. **228–229**, 293 (2005).
[94] J. Meunier, J. Phys. (Paris) **48**, 1819 (1987).
[95] H. Kahl and J. Winkelmann, Fluid Phase Equilib. **270**, 50 (2008).
[96] G. J. Gloor, G. Jackson, F. J. Blas, and E. de Miguel, J. Chem. Phys. **123**, 134703 (2005).
[97] C. McCabe, A. Gil-Villegas, and G. Jackson, J. Phys. Chem. B **102**, 4183 (1998).
[98] C. McCabe, A. Galindo, A. Gil-Villegas, and G. Jackson, J. Phys. Chem. B **102**, 8060 (1998).
[99] C. McCabe, A. Galindo, A. Gil-Villegas, and G. Jackson, Int. J. Thermophys. **19**, 1511 (1998).
[100] C. McCabe and G. Jackson, Phys. Chem. Chem. Phys. **1**, 2057 (1999).
[101] A. Galindo, A. Gil-Villegas, P. J. Whitehead, G. Jackson, and A. N. Burgess, J. Phys. Chem. B **102**, 7632 (1998).
[102] A. Galindo, A. Gil-Villegas, G. Jackson, and A. N. Burgess, J. Phys. Chem. B **103**, 10272 (1999).
[103] G. N. I. Clark, A. J. Haslam, A. Galindo, and G. Jackson, Mol. Phys. **104**, 3561 (2006).
[104] A. Galindo, L. J. Florusse, and C. J. Peters, Fluid Phase Equilib. **158–160**, 123 (1999).
[105] D. P. Visco and D. A. Kofke, Fluid Phase Equilib. **158–160**, 37 (1999).
[106] A. Galindo, S. J. Burton, G. Jackson, D. P. Visco, and D. A. Kofke, Mol. Phys. **100**, 2241 (2002).
[107] A. Galindo and F. J. Blas, J. Phys. Chem. B **106**, 4503 (2002).
[108] F. J. Blas and A. Galindo, Fluid Phase Equilib. **194–197**, 501 (2002).
[109] E. J. M. Filipe, E. J. S. Gomez de Azevedo, L. F. G. Martins, V. A. M. Soares, J. C. G. Calado, C. McCabe, and G. Jackson, J. Phys. Chem. B **104**, 1315 (2000).
[110] E. J. M. Filipe, L. F. G. Martins, J. C. G. Calado, C. McCabe, and G. Jackson, J. Phys. Chem. B **104**, 1322 (2000).
[111] C. McCabe, L. M. B. Dias, G. Jackson, and E. J. M. Filipe, Phys. Chem. Chem. Phys. **3**, 2852 (2001).
[112] R. P. Bonifacio, E. J. M. Filipe, C. McCabe, M. F. C. Gomes, and A. A. H. Padua, Mol. Phys. **100**, 2547 (2002).
[113] E. J. M. Filipe, L. M. B. Dias, J. C. G. Calado, C. McCabe, and G. Jackson, Phys. Chem. Chem. Phys. **4**, 1618 (2002).
[114] L. M. B. Dias, R. P. Bonifacio, E. J. M. Filipe, J. C. G. Calado, C. McCabe, and G. Jackson, Fluid Phase Equilib. **205**, 163 (2003).
[115] A. Gil-Villegas, A. Galindo, and G. Jackson, Mol. Phys. **99**, 531 (2001).
[116] B. H. Patel, P. Paricaud, A. Galindo, and G. C. Maitland, Ind. Eng. Chem. Res. **42**, 3809 (2003).
[117] C. McCabe, A. Galindo, M. N. Garcia-Lisbona, and G. Jackson, Ind. Eng. Chem. Res. **40**, 3835 (2001).
[118] P. Paricaud, A. Galindo, and G. Jackson, Ind. Eng. Chem. Res. **43**, 6871 (2004).
[119] A. J. Haslam, N. von Solms, C. S. Adjiman, A. Galindo, G. Jackson, P. Paricaud, M. L. Michelsen, and G. M. Kontogeorgis, Fluid Phase Equilib. **243**, 74 (2006).
[120] G. N. I. Clark, A. Galindo, G. Jackson, S. Rogers, and A. N. Burgess, Macromolecules **41**, 6582 (2008).
[121] C. G. Gray and K. E. Gubbins, *Theory of Molecular Fluids: Fundamentals (International Series of Monographs on Chemistry No. 9)* (Clarendon, Oxford, 1984).
[122] J. A. Barker and D. Henderson, J. Chem. Phys. **47**, 2856 (1967).
[123] J. A. Barker and D. Henderson, J. Chem. Phys. **47**, 4714 (1967).
[124] T. Boublík, J. Chem. Phys. **53**, 471 (1970).
[125] G. A. Mansoori, N. F. Carnahan, K. E. Starling, and T. W. Leland, J. Chem. Phys. **54**, 1523 (1971).
[126] L. A. Davies, A. Gil-Villegas, and G. Jackson, J. Chem. Phys. **111**, 8659 (1999).
[127] L. A. Davies, A. Gil-Villegas, and G. Jackson, Int. J. Thermophys. **19**, 675 (1998).
[128] T. Lafitte, D. Bessieres, M. M. Pineiro, and J. L. Daridon, J. Chem. Phys. **124**, 024509 (2006).
[129] B. J. Alder and C. E. Hetch, J. Chem. Phys. **50**, 2032 (1969).
[130] N. F. Carnahan and K. E. Starling, AIChE J. **18**, 1184 (1972).
[131] G. Jackson, J. S. Rowlinson, and C. A. Leng, J. Chem. Soc., Faraday Trans. 1 **82**, 3461 (1986).
[132] D. G. Green and G. Jackson, J. Chem. Phys. **97**, 8672 (1992).
[133] D. G. Green and G. Jackson, J. Chem. Soc., Faraday Trans. **88**, 1395 (1992).
[134] A. Galindo, P. J. Whitehead, G. Jackson, and A. N. Burgess, J. Phys. Chem. **100**, 6781 (1996).
[135] J. A. Barker and D. Henderson, Rev. Mod. Phys. **48**, 587 (1976).
[136] T. M. Reed and K. E. Gubbins, *Applied Statistical Mechanics* (McGraw-Hill, New York, 1971).
[137] W. G. Chapman, G. Jackson, and K. E. Gubbins, Mol. Phys. **65**, 1057 (1988).
[138] G. Jackson, W. G. Chapman, and K. E. Gubbins, Mol. Phys. **65**, 1 (1988).
[139] J. P. Hansen and I. R. McDonald, *Theory of Simple Liquids* (Academic, London, 1986).
[140] E. Kierlik and M. L. Rosinberg, J. Chem. Phys. **97**, 9222 (1992).
[141] E. Kierlik and M. L. Rosinberg, J. Chem. Phys. **99**, 3950 (1993).
[142] S. Phan, E. Kierlik, M. L. Rosinberg, A. Yethiraj, and R. Dickman, J. Chem. Phys. **102**, 2141 (1995).
[143] S. Toxvaerd, J. Chem. Phys. **55**, 3116 (1971).
[144] S. Toxvaerd, Mol. Phys. **26**, 91 (1973).
[145] S. Toxvaerd, J. Chem. Phys. **64**, 2863 (1976).
[146] J. R. Henderson, *Statistical Mechanics of Spherical Interfaces in Fluid Interfacial Phenomena* (Wiley, New York, 1986).
[147] M. J. D. Powell, *A Hybrid Method for Nonlinear Equations, Numerical Methods for Nonlinear Equations* (Gordon and Breach, London, 1970).

[148] L. A. Davies, A. Gil-Villegas, G. Jackson, S. Calero, and S. Lago, Phys. Rev. E **57**, 2035 (1998).
[149] R. L. Scott and P. H. van Konynenburg, Discuss. Faraday Soc. **49**, 87 (1970).
[150] P. H. Van Konynenburg and R. L. Scott, Philos. Trans. R. Soc. London, Ser. A **298**, 495 (1980).
[151] K. G. Wilson, Phys. Rev. B **4**, 3174 (1971).
[152] S. Srivastan, N. A. Darwish, K. A. M. Gasem, and L. R. Robinson, J. Chem. Eng. Data **37**, 516 (1992).
[153] R. P. Sear and G. Jackson, J. Chem. Phys. **103**, 8684 (1995).
[154] P. Paricaud, S. Varga, and G. Jackson, J. Chem. Phys. **118**, 8525 (2003).
[155] D. C. Williamson and G. Jackson, J. Chem. Phys. **108**, 10294 (1998).
[156] M. Franco-Melgar, A. J. Haslam, and G. Jackson, Mol. Phys. **106**, 649 (2008).
[157] M. Franco-Melgar, A. J. Haslam, and G. Jackson, Mol. Phys. **107**, 2329 (2009).